CHALMERS
UNIVERSITY OF TECHNOLOGY

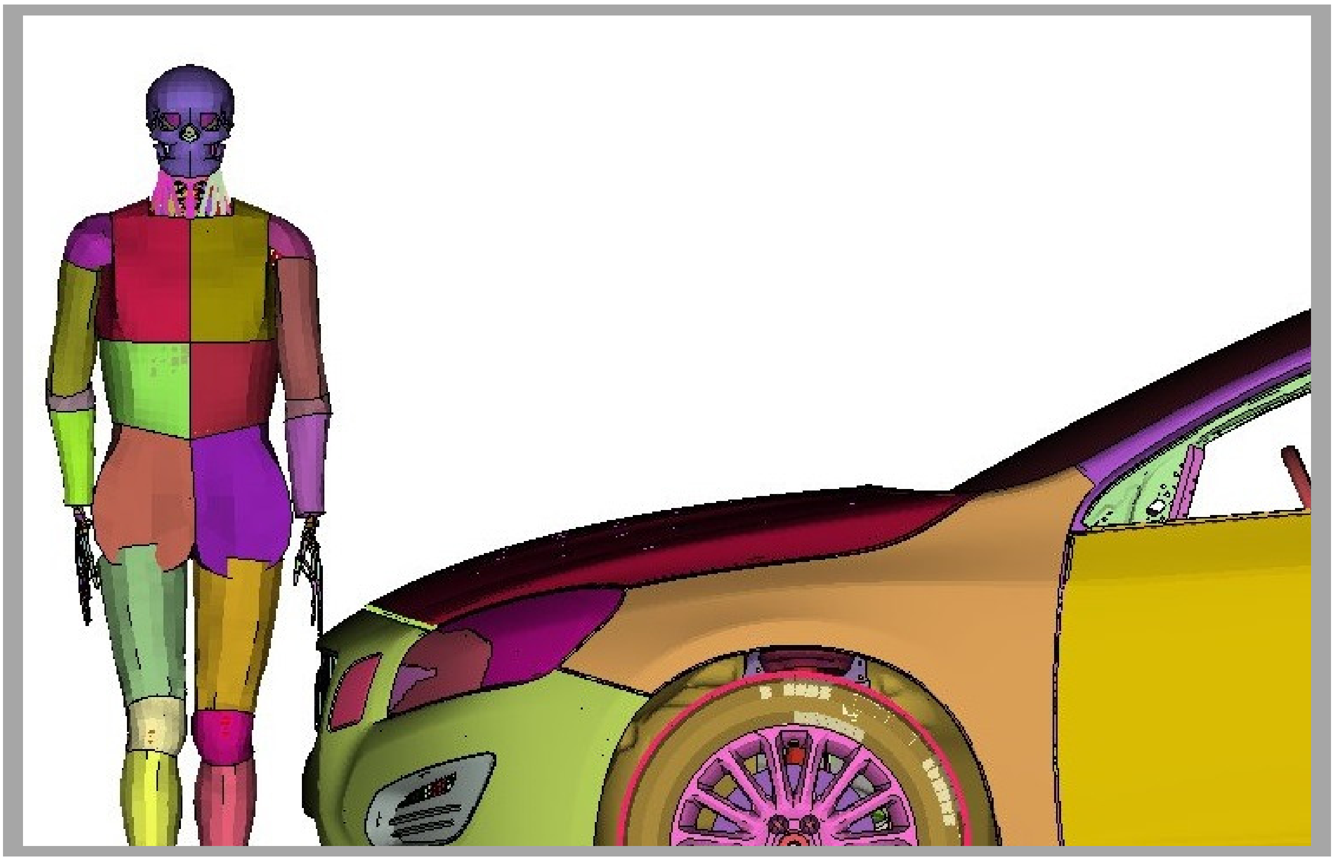

Assessment of injuries to the lower leg and head of pedestrians in vehicle-to-pedestrian collisions through FE simulations

Master's thesis in Automotive Engineering

Pradeep Farkya, XiaoXiao Cheng

Department of Applied Mechanics
CHALMERS UNIVERSITY OF TECHNOLOGY
Gothenburg, Sweden 2015

MASTER'S THESIS IN AUTOMOTIVE ENGINEERING

Assessment of injuries to the lower leg and head of pedestrians in vehicle-to-pedestrian collisions through FE simulations

Pradeep Farkya, XiaoXiao Cheng

Department of Applied Mechanics
Division of Vehicle Safety
CHALMERS UNIVERSITY OF TECHNOLOGY
Göteborg, Sweden 2015

Assessment of injuries to the lower leg and head of pedestrians in vehicle-to-pedestrian collisions through FE simulations
Pradeep Farkya, XiaoXiao Cheng

Master's Thesis 2015: 92
ISSN 1652-8557
Department of Applied Mechanics
Division of Vehicle Safety
Chalmers University of Technology
SE-412 96 Göteborg
Sweden
Telephone: + 46 (0)31-772 1000

Cover:
Image from a LS-DYNA simulation conducted by Authors.

Reproservice / Department of Applied Mechanics
Göteborg, Sweden 2015-10-29

Assessment of injuries to the lower leg and head of pedestrians in vehicle-to-pedestrian collisions through FE simulations
Master's thesis in Automotive Engineering
Pradeep Farkya, XiaoXiao Cheng
Department of Applied Mechanics
Division of Vehicle Safety
Chalmers University of Technology

Abstract

In this thesis an analysis of predicted injuries to the lower leg and head of pedestrians in vehicle-to-pedestrian collisions through finite element (FE) simulations were analyzed. Today, pedestrian regulatory tests consist of subsystem tests using impactors that are made to hit the vehicle; there is no use of any pedestrian crash test dummy. Hence, the kinematics of the impactors used in the testing procedure can be questioned. An alternative way to assess vehicle-to-pedestrian interaction and injury risks is through the use of a FE-Human Body Model (HBM). This thesis presents a comparison of injuries predicted by simulated regulatory tests and injuries predicted by a modified Total Human Body Model for Safety (THUMS), with KTH head and neck model, when impacting an advanced FE-model of a sedan passenger car. The injuries in focus are those sustained to the lower extremities, mainly to the knee ligaments and tibia bone fracture, and the head. Further, real-life vehicle-to-pedestrian accidents were reconstructed with the modified THUMS to indicate the power of accident reconstructions using FE simulations.

The modified THUMS and the leg impactor did not predict similar risk of leg injuries. THUMS predicted lower ligament elongation and higher tibia bending moments than the impactor. The ligament elongation difference between THUMS and impactor is not comparable. For tibia bending moments, THUMS predicted 18% higher bending moments than impactor for impact point P3 and tibia-2 cross-section for small passenger vehicle-to-pedestrian collision, on average it was 60% higher for Flex-PLI positioning 75mm above ground and 42% higher when Flex-PLI is positioned according to THUMS walking stance. For tibia injury risk as predicted with modified THUMS, vehicle velocity and pedestrian impact location along the width of the energy absorber were significant. Moreover, presence of a femur fracture influenced the tibia bending moment; femure fracture varied as a function of impact location and vehicle velocity.

The injuries to the head as predicted by the modified THUMS, with Rigid KTH head and neck model, and headform impactor were found to have similar head impact kinematics with similar head impact duration and behavior of acceleration curve. Predicted head injuries, using the injury measures HIC_{15} and BRIC, were influenced by the head impact location on the vehicle, vehicle height in relation to THUMS and vehicle velocity. In the accident reconstructions modified THUMS model predicted high HIC_{15} values, representing high risk of head injuries as compared to the head injury reported in the two cases that were reconstructed. The difference is qualitative only, no quantitative difference conclusion can be drawn from the results. This deviation in results could be explained due to the fact of non-availability of head impact locations in the database cases, not including the vehicle deceleration which may be present during actual accident and non-inclusion of road and weather conditions.

Keywords: THUMS, KTH head, Flex-PLI, vehicle-to-pedestrian simulations, impactor-to-vehicle simulations, positioning, legform, headform, accident reconstruction.

Contents

Preface

This thesis has been carried for Master's degree in automotive engineering at Chalmers University of Technology. The work has been performed at Volvo Cars Safety Centre and at SAFER. All simulations have been carried out at Volvo Cars. We thank our supervisors at Volvo Cars, Ulf Westberg and Peter Blum for their continued support throughout the course of the thesis work. Also, we thank our examiner Johan Davidsson and Stefan Larsson who have provided us with their expert guidance in the field.

Göteborg 2015-10-29

Pradeep Farkya, XiaoXiao Cheng

Nomenclature

Abbreviations

NHTSA	National Highway Traffic Safety Administration
Euro NCAP	European New Car Assessment Programme
HBM	Human Body Models
FE	Finite Element
PV	Passenger Vehicle
KTH	Kungliga Tekniska Högskolan
AIS	Abbreviated Injury Scale
THUMS	Total Human Body Model for Safety
EEVC	Enhanced European Vehicle Committee
BSRL	Bonnet Side Reference Line
BLE	Bonnet Leading Edge
WAD	Wrap Around Distances
ATD's	Anthropometric Test Devices
PMHS	Post Mortem Human Subjects
Flex-PLI	Flexible Pedestrian Legform Impactor
TRL-LFI	TRL-Legform Impactor
AAAM	Association for the Adavancement of Automotive Medicine
ISS	Injury Severity Score
ACL	Anterior Cruciate Ligament
PCL	Posterior Cruciate Ligament
MCL	Medial Collateral Ligament
CSF	CerebroSpinal Fluid
HIC	Head Injury Criteria
BrIC	Brain Rotational Injury Criteria
MPS	Maximum Principal Strain
AM50	Adult Male 50th percentile
AF05	Adult Female 5th percentile
AM95	Adult Male 95th percentile
CT	Computer Tomography
V_PAD	Volvo Pedestrian Accident Database
NCPU	Number of Central Processing Units
ANMC	Approximate Natural Movement Curve

IMVITER	Implementation of Virtual Testing in safety Regulations
CFC	Channel Frequency Class
DAI	Diffuse Axonal Injury
CSDM	Cumulative Strain Damage Measure
RIC	Rotational Injury Criteria
N	Reference case for normalization

Notations

a(t)	Acceleration as a function of time
dt	time interval (s)
t1	Time at initial head impact (s)
t2	Time at rebound of head (s)
ω_x	Angular velocity in x-direction (rad/s)
ω_y	Angular velocity in y-direction (rad/s)
ω_z	Angular velocity in z-direction (rad/s)
ω_{xc}	Critical Angular velocity in x-direction (rad/s)
ω_{yc}	Critical Angular velocity in y-direction (rad/s)
ω_{zc}	Critical Angular velocity in z-direction (rad/s)

Anatomical Abbreviations

Anterior	Towards the front
Posterior	Towards the back
Distal	Further away from the torso
Lateral	Sideways

1 Introduction

Today, traffic accidents are one of the leading causes of injuries and fatalities. While it is important to ensure better safety for vehicle occupants, it is equally important to ensure that other vulnerable road users like pedestrians and bicyclists are protected as well from vehicle collisions. According to statistics in 2012 in U.S, 4,743 pedestrians and 726 bicyclists were killed in crashes with motor vehicles [1]. As supported by statistics from National Highway Traffic Safety Administration (NHTSA), though, the number of pedestrian fatalities fell from 4,901 in 2001 to 4,743 in 2012, there were still 76,000 reported pedestrian injuries in 2012 [1], which refers to high number of pedestrian injuries. To conclude, pedestrian protection is still of major concern for the society and for the vehicle industry.

In Europe, around 70% of all vehicle-to-pedestrian interactions involve a passenger vehicle [2]. A pedestrian is usually struck with the vehicle front while walking or running rather than standing still and the vehicle-to-pedestrian impact kinematics are greatly influenced by the stance of the pedestrian [2]. The pedestrian commonly sustain injuries to the lower leg and head. The injury risk appear to be a function of vehicle velocity, vehicle height and impact location. Improved understandings of pedestrian kinematics and injury risk are of significant interest as this information can be useful in vehicle development.

European New Car Assessment Programme (Euro NCAP) uses Flex-PLI legform and headform impactor to assess the risk of injuries to the lower leg and head of a pedestrian in the event of a collision [3]. However, the current NCAP testing involves only subsystem testing. Detailed kinematics and more precise injury predictions could be obtained using finite element (FE) Human Body Models (HBM) and could be a useful tool in the development of safer vehicles. Moreover, by using HBMs and finite element (FE) simulations it is possible to carry out parameter studies and analyze injuries without the need to conduct large volume real crash tests with a crash test dummy, thus saving money for the manufacturer.

For this study, the vehicle used was a small passenger vehicle (PV), the HBM used was the Total Human Body Model for Safety (THUMS) developed by Toyota Motor Labs [4] that was fitted with the advanced head and neck model from Royal Institute of Technology (KTH) [5]. The combined model in this thesis is referred to as the THUMS KTH model.

Objectives

The objectives were the following:

1. Compare the risk of pedestrian leg and head injuries as predicted by simulations of the Euro NCAP sub-system tests and those predicted by the THUMS KTH model.
2. Study injuries to the lower leg and head of THUMS in vehicle-to-pedestrian collisions and analyse the influence of vehicle velocity, vehicle height and pedestrian impact location on the risk of injuries.
3. Assess the feasibility of reconstructions of real-world accidents.

2 Background

This section provides the reader with a summary of the theoretical concepts which govern the work carried out in this thesis. In this section general knowledge about vehicle-to-pedestrian interactions, details about the lower leg and head test methods as used in Euro NCAP, the design of the abbreviated injury scale (AIS), injury biomechanics, criteria and risk functions concerned with lower leg and head, the design of the Total Human Body Model for safety (THUMS) are presented. Finally, a presentation of the Volvo Pedestrian Accident Database (V_PAD) is introduced.

2.1 Vehicle-to-pedestrian interactions

Vehicle-to-pedestrian interactions refers to the scenario in which pedestrian is impacted by vehicle before, during and after the collision. Knowledge about vehicle-to-pedestrian interactions can be based on reports from police or hospital. But, there is commonly no information in these reports about the pedestrian stance and impact locations on vehicle. Another source of such information is from research institutes or industrial in-house accident research. One such study is from Lindman et al. [6], where out of 314 identified cases 179 cases were those in which the vehicle was moving forward which means 57% cases represented a vehicle moving forward without turning. Also, in 66% of these cases the pedestrian was crossing in front of the vehicle facing either to the left or right direction relative the vehicle. In 70% of these cases the pedestrian was walking or running while being hit by a vehicle. The data show that a pedestrian is likely to be impacted by a vehicle in walking position rather in standing position or facing towards the vehicle.

When a vehicle hits a pedestrian, the bumper first impacts with the lower extremities then the upper body rotates around the torso, after which the upper extremities rotate and impact with the vehicle bonnet following impact of head with either bonnet or windshield depending on vehicle geometry, vehicle velocity and height of the pedestrian (Figure 2.1). Lindman et al. [6] also analysed the severity of frequently injured body regions among pedestrians according to Abbreviated Injury Scale (AIS). According to the study, in 34% of the cases, the pedestrian had AIS2+ injury level for lower extremities whereas in 24% of the cases there was AIS2+ head injury level [6]. So, the lower extremities and head are most frequently injured body parts of pedestrians during vehicle-to-pedestrian collisions.

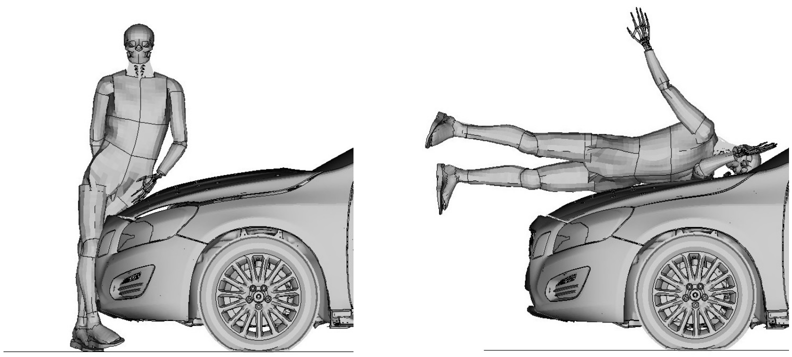

Figure 2.1: FE-simulation of a pedestrian collision to indicate vehicle-to-pedestrian interactions; leg impact (left) and head impact (right) for small passenger vehicle.

Vehicle-to-pedestrian interactions could be studied by sub-system testing using impactors, testing using ATD's and PMHS tests. As of now, regulations like NCAP [3] for vehicle pedestrian safety include sub-system testing while full-scale dummy testing and PMHS tests are rare. Subsystem testing using impactors is easy to conduct but it doesn't necessarily represent the actual kinematic behaviour of living human being during a collision. An attractive alternative are the used of FE-HBMs. FE models of pedestrian have been found to be more bio-fidelic than impactors or dummies [7] and thus using computer simulations a parametric study is easy to perform and could be made more repeatable.

2.2 Euro NCAP

Euro NCAP is a voluntary vehicle safety rating system founded by seven governments as well as several transportation agencies in European countries in 1997 [8][9]. When NCAP was introduced it made use of a five star rating system; a safety performance scale from good to poor. This was done for particular aspects as well as the overall performance. Such system aims to help the customer to better understand the safety performance of a vehicle [10].

From year 2009, Euro NCAP increased its attention on the pedestrian protection provided by a vehicle, thus a new pedestrian vehicle safety assessment program was proposed. The pedestrian NCAP program addresses the safety of adults, children and addresses safety assist technologies [11]. The assessment protocol, partially based on test methods and biomechanics threshold provided by the European Enhanced Vehicle-safety Committee (EEVC), that is currently in use was released in June 2014 [12] [13]. It includes impacts to the vehicle evaluated using an adult headform, a child headform, an upper legform and a lower legform [14]. Even though different vehicle shapes and categories may lead to variant impact velocity and angle, EEVC claimed that such standard test is a compromise but also a feasible way [14].

Unlike the real-life where the vehicle hits a pedestrian, in an EEVC sub-system test the vehicle is stationary and the impactor is made to hit the vehicle at a speed of 40 km/h. The tests can be seen in Figure 2.2.

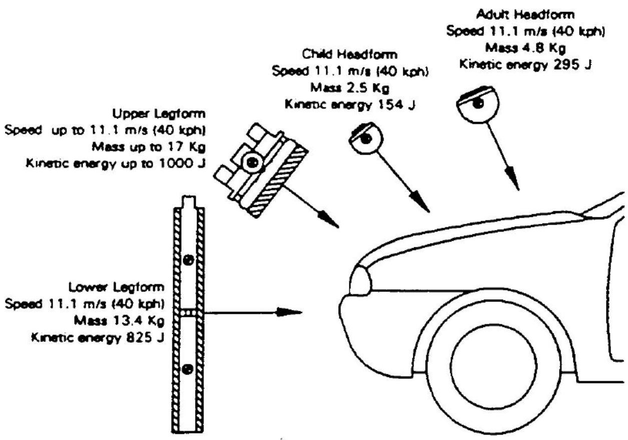

Figure 2.2: A summary of EEVC pedestrian protection test methods [14]

2.2.1 Vehicle marking

Euro NCAP pedestrian protocol describe a vehicle marking system that is used to prepare and analyse the tests. By implementing such procedure, a test vehicle can be described by different impact zones which makes it possible to locate the respective interaction points and select the appropriate impactor conditions.

2.2.1.1 Bonnet Side Reference Lines

The Bonnet Side Reference Lines (BSRL) are used to identify the border between the side and the bonnet of the vehicle. A straight edge of 700 mm long is placed at 45°to the vertical plane and moved along the side wing of a vehicle. The uppermost point on the vehicle contacting between the straight edge and bonnet is marked. The BSRL is then created by joining all the marked points to predict the outermost edge along the vehicle bonnet width. Such drawing should be performed on both sides of the vehicle. Figure 2.3 shows an example of a BSRL on one side of a vehicle.

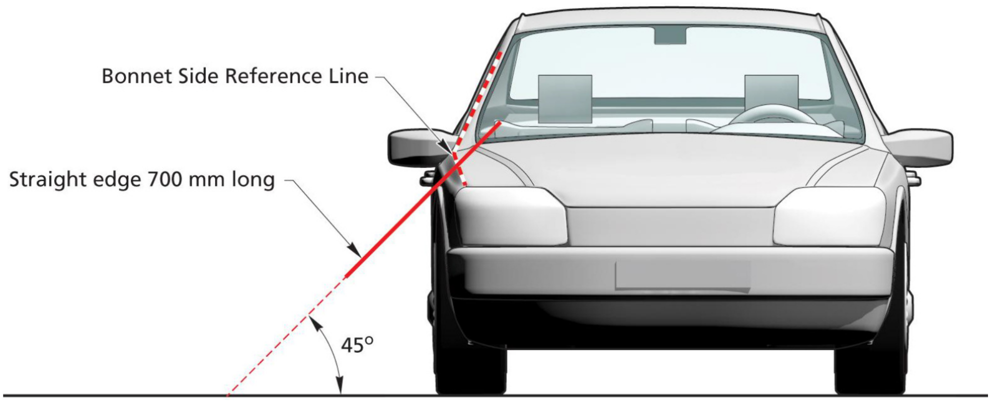

Figure 2.3: Vehicle BSRL marking on the right side [12]

2.2.1.2 Bonnet Leading Edge Reference Line

The Bonnet Leading Edge Reference Line identifies the front surface of the bonnet. It marks the uppermost and outermost surface of the vehicle front. For drawing this, a straight edge of 1000 mm long is used and placed at 600 mm above the ground level then lend to the vehicle at 50° to the vertical plane (Figure 2.4). The lowest contact points between the straight edge and the vehicle front are marked and joined to shape the Bonnet Leading Edge (BLE) Reference Line. The vertical distances between the BLE and the ground plane is referred to as BLE height (Figure 2.4). The BLE usually has great influence on pedestrian's femur injury as it attempts to be the first contact region between human's upper leg and the vehicle exterior. In this study, the BLE is used to determine the classification of vehicle in chapter 3.3.

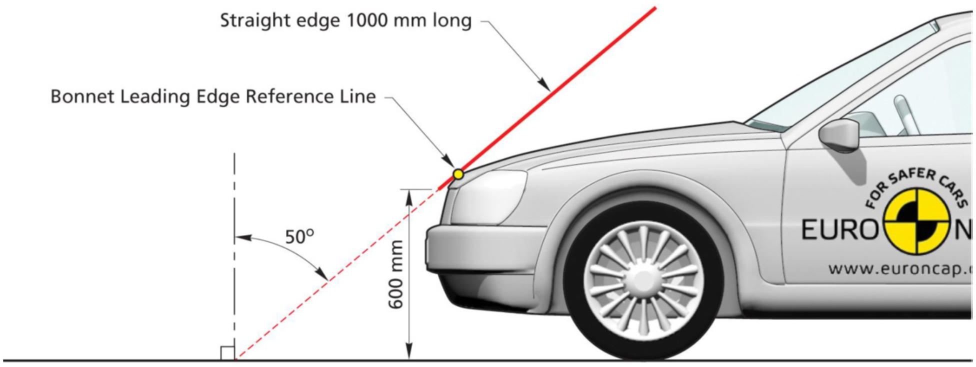

Figure 2.4: Determination of BLE height as described by Euro NCAP [12]

2.2.1.3 Wrap Around Distance and Grid Points

The head Wrap Around Distance (WAD) is used in the Euro NCAP protocol to determine the test area and the selection of a headform size; adult or child headform. The measurement of WAD is from the ground level, wraps the outer vehicle surface using a flexible tape, to the head impact point. The head impact point can be on the bonnet or windshield. Commonly the WAD is measured between the vehicle centreline and the wings with the boundary defined by the BSRL; all the points having the same WAD make up for a WAD line. The zone between a WAD of 1000 mm and 1500 mm are to be tested with a child headform and the zone between 1700 mm and 2100 mm is to be tested with the adult headform. The impactor selection between 1500 mm and 1700 mm is determined by the location of the bonnet rear reference line (BRRL), which defines the rear range of the bonnet. The child impactor or the adult impactor will be used in the 1500 mm to 1700 mm zone if the BRRL is rearward of 1700 mm or forward of 1500 mm. When the BRRL is between 1500 mm and 1700 mm, points forward of it will be assessed using a child impactor while points rearward will be using an adult impactor.

Grid Points are the target locations for the headform impacts. To perform such marking procedure, firstly the target points are picked at the centreline every 100mm from 1000mm WAD to 2100mm WAD, then use the same 100mm interval to mark on the vehicle surface laterally from the points that are created in the first step. Target points are labelled according to the impact zone, and the head impactor should be selected respectively (Figure 2.5).

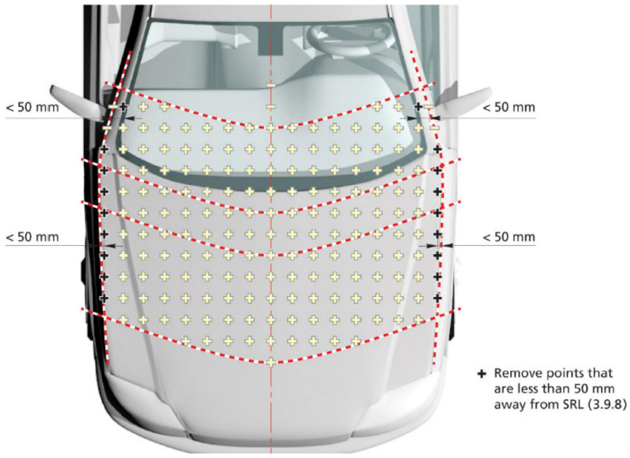

Figure 2.5: WAD lines and Grid Points as defined by Euro NCAP [12]

Generally, target points start with 'C.' indicating the testing location is suitable for a child/small headform, while a grid point for adult headform starts with 'A.' along with a number identifying the location.

2.2.2 Sub-system tests

A full-scale test with a pedestrian crash test dummy, also referred to as an anthropomorphic test device (ATD), is difficult to implement in a pedestrian assessment protocol because of its limited reproducibility. Therefore, test protocols that include sub-system test devices have been adopted by most of the rating organizations or regulatory bodies, including Euro NCAP. In EEVC reports, the design specifications of the impactors and the strategy of implementation in the test were suggested. Test methods and injury risk functions/thresholds of these impactors were provided from reconstructions of real-world accidents and from Post Mortem Human Subjects (PMHS). The latest impactor design recommended of EEVC came in 1999 with a further improvement in terms of biofidelity. However, Euro NCAP and other organizations tend to pursue more realistic tests thus the updates of the impactor designs have been suggested.

2.2.2.1 Legform to bumper test

The impactor is commonly referred to as the TRL Pedestrian Legform Impactor (TRL-LFI) which consists of two rigid parts and a flexible joint that are to resemble the femur, the tibia and the knee, respectively (Figure 2.6). According to the EEVC proposal [14], a legform to bumper test should be carried out at least at three different impact positions; where there are highest risk of injuries. The impactor is set to hit the vehicle front laterally with an impact velocity of 11.1 m/s, and the instrumentation under consideration are the tibia bending measured by the bending moment at four locations and the knee bending measured by the elongation of three ligaments in the knee joint. The test points are selected with certain limitations of the distance between each other and to the defined edge of the bumper corner [14]. Recently, the new Flexible Pedestrian Legform Impactor (Flex-PLI) was recommended for the updated Euro NCAP pedestrian protection test [14] (Figure 2.6). Compared to the EEVC-legform , the Flex-PLI has a more anthropomorphic behaviour as both the unit representing the upper leg (femur bone) and the unit representing the lower leg (tibia bone) are flexible.

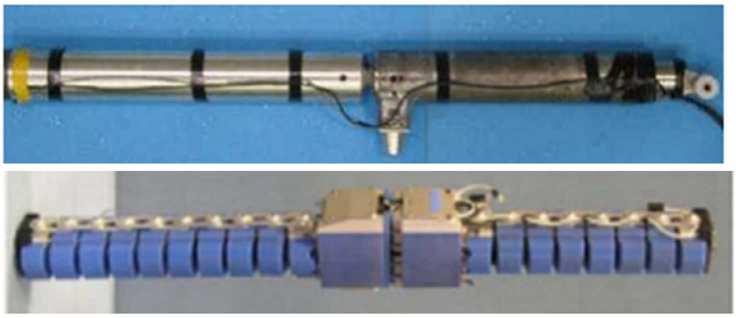

Figure 2.6: Photos of the load carrying units (without padding) of the TRL-LFI based on EEVC WG 10/WG17 (top) [15] and of the Flex-PLI version GTR (bottom) [16]

2.2.2.2 Headform to bonnet top test

The headform impactor specification and the test method of Euro NCAP pedestrian assessment conform to the Regulation (EC) 78/2009 and Regulation (EC) 631/2009 as a supplement. The adult headform should be released at a speed of 11.1 m/s and an angle of 65°±2°to the ground. In the child headform test, the speed is the same as in the adult test while the angle shall be 50°±2° to the ground [12]. The vehicle manufacturer is required to provide test results of the child/small headform and the adult headform on each grid point that is pre-defined by the boundaries of WAD lines and different impact zones. The performance criteria, the HIC_{15} or the colour data showing the severity, is obtained from the accelerometer installed at the centre of gravity of the headform.

2.3 FE- Human Body Models

The FE-Human Body Models are used in vehicle safety simulations for pedestrian or occupant protection owing to the advantage of being variable and repeatable as a biofidelic numerical tool. The modelling contains bones and soft tissues like flesh, skin and ligaments using numerical methods. The widely used total HBMs include the

General Motors (GM)/ University of Virginia (UVA) model, Human Model for Safety (HUMOS) model, Global Human Body Models Consortium (GHBMC) model and the model under study, the THUMS model. This chapter is going to introduce these models with emphasis on THUMS.

2.3.1 GM/UVA model, HUMOS model and GHBMC model

The GM/UVA model was developed and validated by the University of Virginia. This model has the size of a 50th percentile male with the geometry data from a United States institution [17]. The model HUMOS was first released in 2001 with a sitting posture represented as the occupant position. It contains about 50000 elements to model the bones, skin, muscle, ligaments and internal organs. A study by Tropiano et al. tested the HUMOS model in a whiplash situation. The result showed good correlation with the clinical and experiment data [18]. An advanced version, HUMOS 2, was released in the year 2006 together with a tool to facilitate size scaling and positioning. The GHBMC model was developed by GHBMC, a consortium sponsored by several international institutions and vehicle manufacturers. The 50th percentile male model reproduced a 26 years old male with 78.6 kg in weight and 175cm in height. The consortium has planned to scale the model into different age, sex and height. A standing posture was also submitted to Euro NCAP.

2.3.2 THUMS

The THUMS is a computational model developed by Toyota Motor Corporation and Toyota Central R&D Labs since from 1997. The aim of the THUMS model is to enable an investigation of the human kinematics and injuries in the vehicle safety domain. Comparing to crash test dummies, THUMS has the merit of being more anthropomorphic and includes soft tissues, a skeleton system, and internal organs. THUMS model comes in two postures, one to represent occupant in sitting posture and another to represent a pedestrian in standing posture. The size is that of a 50th percentile adult male (AM50). THUMS is currently available in versions 1, 3 and 4. THUMS version 4 is also developed to be representative of a 5th percentile adult female (AF05) and a 95th percentile adult male (AM95).

2.3.2.1 THUMS AM50 Pedestrian Model Version 1.4

The THUMS AM50 Pedestrian Model, Version 1.4 (hereinafter called THUMS v1.4) was released in 2006 and is simpler model as compared to more recent versions. Figure 2.7 shows the main components of the THUMS v1.4.

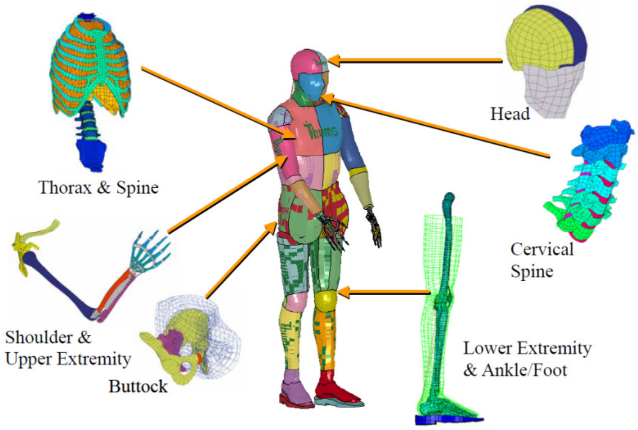

Figure 2.7: Components of THUMS v1.4 [19]

The general behaviour of THUMS v1.4 have been reported to be humanlike [20]. A study by Yasuki et al. [21] reconstructed several PMHS tests by THUMS v1.4 and an SUV FE model and drew the conclusion that the kinematics of pedestrian FE model, THUMS v1.4, and its injury prediction to the lower leg showed good correlation with the PMHS test. A general description of THUMS v1.4 model on both anthropomorphic properties and FE outline are listed in the Table 2.1.

Table 2.1: Description of THUMS v1.4, from the THUMS v1.4 user's guide [19]

Anthropomorphic property	
Male Height: 175cm Weight: 77kg Age: 30 to 40 Stance: Standing posture	
Finite Element property	
Total number of Nodes : 63,300 Total number of Elements: 81,5000	
Tissue type	Typical element type
• Muscle • Tendon	Beam element
• Skin • Cortical Bone • Ligament	Shell element
• Spongy Bone • Disc • Internal Organ • Brain	Solid element

In detail, the head of THUMS v1.4 is made of 8,100 elements, whereas the brain is modelled as a whole part. Such specification cannot support any in-depth analysis of brain injury for the reason that this simplified head cannot match with the complexity of a human skull and brain. For this reason, a more advanced head design was fitted the THUMS v1.4 which will be introduced in the subsequent section.

2.3.2.2 THUMS KTH model

KTH developed a FE head and neck model from computer tomography (CT) images, and a simpler model by replacing the brain with a less detailed and more solid brain. The neck includes cervical vertebras and discrete springs to represent the neck muscles, which is implemented in both models. These two models were attached to an AM50 pedestrian THUMS model version 1.4 to facilitate improved kinematic behaviour during vehicle-to-pedestrian collisions and injury predictions. Figure 2.8 provides the FE model of the detailed head and neck with the brain exposed. Such brain model was validated by Kleiven et al. [22] [23]. In this report, both THUMS KTH model with advanced head and THUMS KTH model with rigid head will be used and compared further.

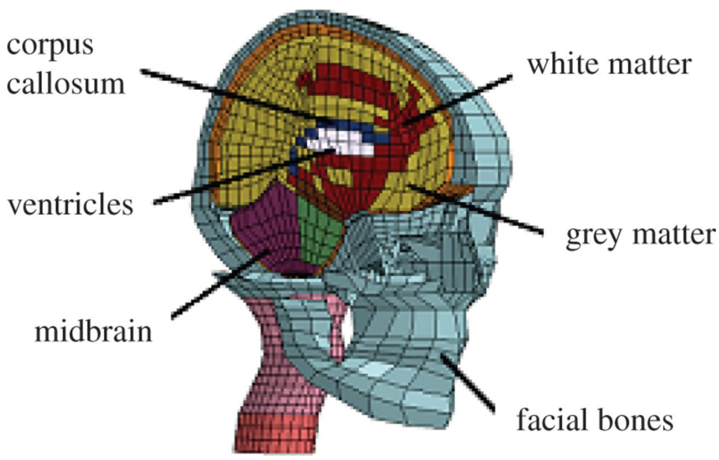

Figure 2.8: The KTH detailed head model (Source: Giordano et al. [24])

2.4 Abbreviated Injury Scale (AIS)

AIS is an anatomical scoring system which was first introduced in 1969 [25]. The AIS is monitored by a scaling committee of the Association for the Advancement of Automotive Medicine (AAAM). In this scoring system, the injuries are ranked from 1 to 6, with 1 being minor and 6 a maximal injury. This only represents the threat to life associated with an injury, to know the severity associated with an injury, another criteria named Injury Severity Score (ISS) is used which is based on AIS. Table 2.2 shows AIS score and corresponding injury level.

Table 2.2: Abbreviated Injury Scale (AIS) levels

AIS score	Injury
1	Minor
2	Moderate
3	Serious
4	Severe
5	Critical
6	Maximal

AIS coding is done with reference to the injuries corresponding to each level in that body region. Details about this are found in the AIS chapters on different body regions [26].

2.5 Biomechanics

Biomechanics can be described as *the application of engineering principles to the study of forces and motions of biological systems [27]*. Thus, biomechanical studies are used to determine the magnitude and direction of forces and moments of various tissues and measure the corresponding kinematics [27]. Further, such studies can be used to determine accelerations associated with rigid and soft regions of the body like head and brain [28].

2.5.1 Lower leg

The study involves analyzing the injuries sustained by a pedestrian to the lower leg which includes the ligament injuries in the knee and fractures of the tibia bone in the leg. The anatomy of the lower limbs of a human is shown in Figure 2.9.

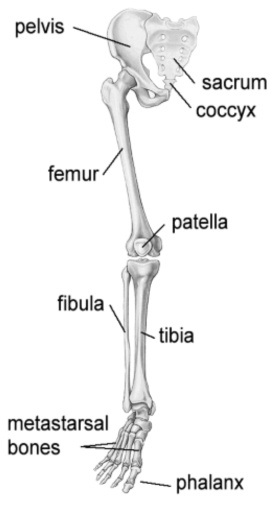

Figure 2.9 Anatomy of lower extremities of a human being [29]

The lower limbs consists of pelvis, thigh, knee, lower leg, ankle and foot. Pelvis links the lower extremities to the spine and it is composed of four bones, two are the hipbones which form the side and the front walls while the sacrum and coccyx form the rear wall. Femur is the long bone of the thigh and is proximally connected by the hip joint to the pelvis and distally linked to knee [29]. The lower leg consists of fibula and tibia between the knee and ankle. The knee is the joint that connects the femur and lower leg and it consists of muscles, tendons, ligaments and menisci. Finally, the foot is adjoined to the lower leg and it consists of several bones [29]. The lower leg bones are subjected to forces and moments during an event of collision with a vehicle.

The anatomy of knee joint of a human is as shown in Figure 2.10.

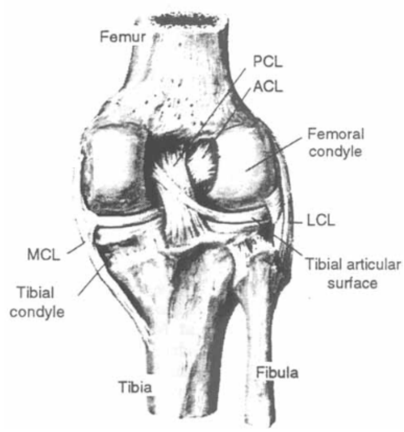

Figure 2.10 Ligaments of the knee of a human being [29]

The four knee ligaments which are frequently injured during collision with vehicle are anterior cruciate ligament (ACL), posterior cruciate ligament (PCL), lateral collateral ligament (LCL) and medial collateral ligament (MCL). The injury happens mainly due to overloading in restricted abnormal joint motion.

2.5.1.1 Lower leg injury mechanism and injury criteria

During vehicle-to-pedestrian impacts, femur, knee-patella, tibia, fibula and foot bone fractures are common. Also knee ligaments rupture occur frequently; especially the collateral ligament [29]. Tibia fractures occur between the mid-shaft region and the distal-third of the tibia where its cross-section is small. A more severe tibia injury is tibial plateau fracture, i.e. a fracture of upper most part of the tibia. It involves a disrupture of the articular surface of the knee-joint.

For knee ligaments, the elongation of the ligaments is used as injury assessment criteria. MCL elongation is considered to predict knee bending angle while ACL and PCL are for the knee shear displacement measurement. For tibia fracture, tibia bending moment measured at different tibia cross-sections is used as an injury criteria as this is measured both in leg form and HBM. Details on the tibia cross-sections are introduced in section 3.3.

For assessing the risk of fracture (%) of the mid-tibia section, the following risk curve in which risk of fracture is a function of bending moment is used for the study (Figure 2.11). The risk curve has been geometrically scaled for moment.

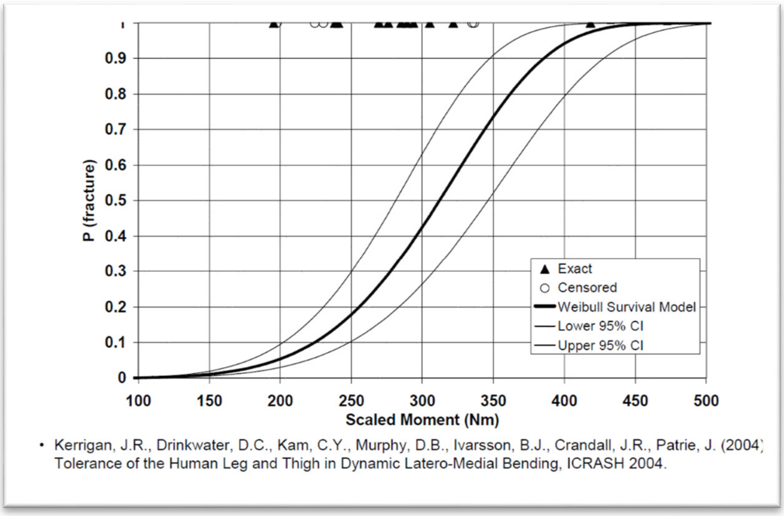

Figure 2.11: Risk curve for probability of fracture for mid-shaft of lower leg [30].

2.5.2 Head

When a vehicle hits a pedestrian, depending on the speed of vehicle and height of the pedestrian, the head of the pedestrian impacts either the bonnet or windshield. Thus, studying the injuries sustained to the head during vehicle-to-pedestrian collisions is very interesting especially when injuries to head could lead to life-long health implications on human beings. Such study is also useful for vehicle industry during vehicle development stage where measures to prevent head injury could be introduced.

The anatomy of human head is as shown in Figure 2.12.

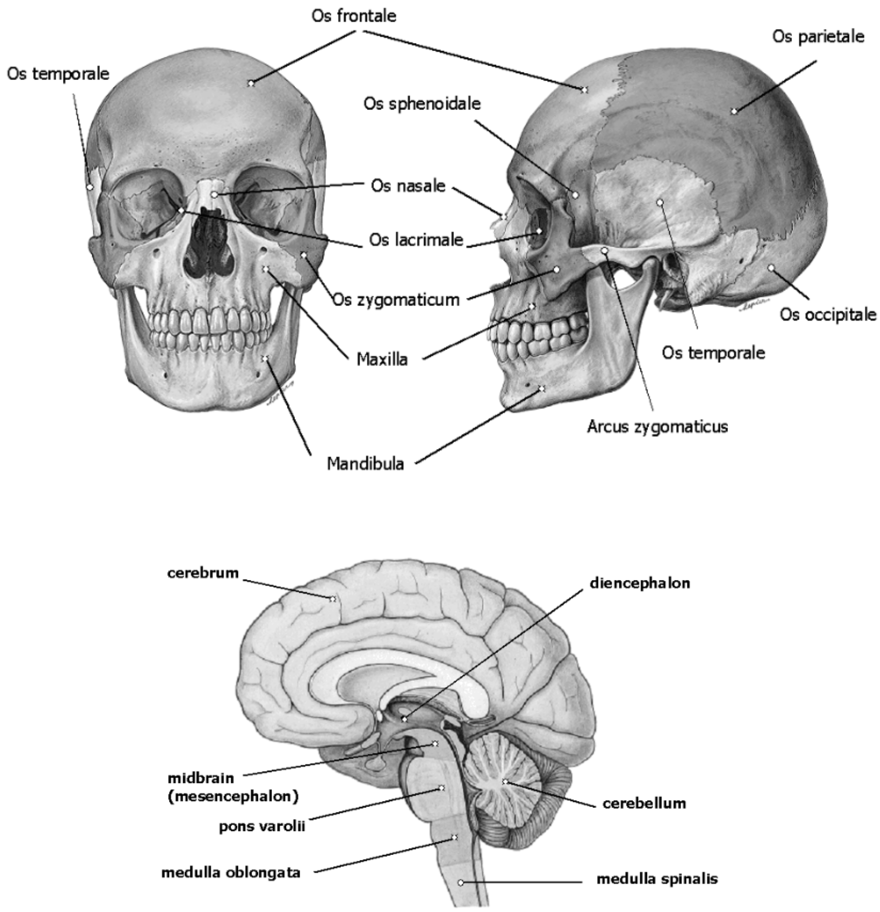

Figure 2.12: Anatomy of head of a human being (top), Brain Anatomy (bottom) [29]

The human head is a multi-layered structure with scalp as outermost layer, followed by skull, the meninges and the brain. The scalp is a thin subcutaneous connective tissue layer surrounding the skull [29]. Skull consists of several bones fused together. The meninges support and protect the spinal cord and the brain and it also has the Cerebrospinal fluid (CSF) which is a dampening fluid helping to protect injuries to brain.

The most important injuries which is of concern to a pedestrian during an event of impact are to the skull and brain. Scalp injuries which are common in automotive accidents include contusion and laceration [29]. Skull injuries can be due to fracture of the skull or soft tissue injury to the brain. Brain injury on the other hand, can be focal brain injury or diffuse brain injury which can be classified further [29]. Brain injuries that occur frequently and of concern are concussions and diffuse axonal brain injuries. Apart from this focal brain injuries which include contusions and hematoma are also common in vehicle-to-pedestrian accidents.

2.5.2.1 Head injury mechanism and injury criteria

Injury mechanism of head injuries in vehicle-to-pedestrian accidents are mainly due to dynamic loading. In dynamic loading there are two types, contact and non-contact loading. Contact loading can cause focal injuries like skull fractures and head local brain injury like contusion. In non-contact loading, acceleration of the head which include translational and rotational acceleration can lead to diffuse brain injuries.

Head Injury Criteria (HIC) is commonly used to assess the injuries to the skull and brain in current regulatory testing in Euro NCAP and vehicle industry pedestrian safety testing. However, there is a limitation to the assessment of brain injuries as rotational accelerations and velocities are not included in calculation of HIC. Thus, it could only represent the assessment of injuries caused due to linear loading. HIC is computed based on the following expression:

$$\mathrm{HIC} = \left\{ \left[\frac{1}{t2 - t1} \int_{t1}^{t2} a(t)dt \right]^{2.5} (t2 - t1) \right\}_{max}$$

HIC value is either calculated for an impact duration of 36ms named as HIC_{36} or for a duration of 15ms named as HIC_{15}. The threshold value of HIC_{36} and HIC_{15} above which severe head injuries occur are 1000 and 700 respectively [29]. The HIC_{15} and head injury risk (%) variation for AIS2+ and AIS3+ is shown in Figure 2.13.

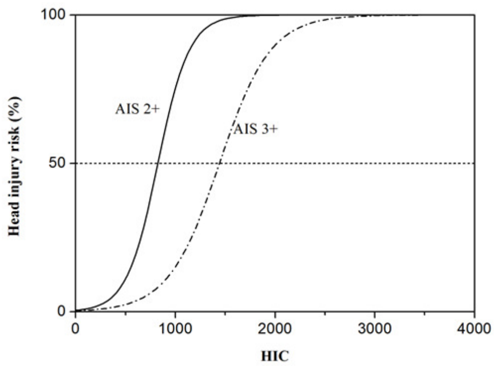

Figure 2.13: Head injury risk curve for AIS2+ and AIS3+ based on HIC15 values [31].

Brain Injury Criterion (BrIC) is a rather new brain injury assessment criteria developed by Takhounts et al (2013) which is complimentary to the HIC. It takes peak head rotational velocities in three components into account. BrIC has been developed for ATD's including Hybrid III 50% male and is based on reconstructions of animal injury data [32]. BrIC is rather a new injury criteria and the use of the same for an advanced FE model like THUMS is further investigated in the thesis.

BrIC is computed based on the following expression:

$$BrIC = \sqrt{\left(\frac{\omega_x}{\omega_{xC}}\right)^2 + \left(\frac{\omega_y}{\omega_{yC}}\right)^2 + \left(\frac{\omega_z}{\omega_{zC}}\right)^2}$$

Takhounts et al. proposed the risk curve equations in their report and the formulation of AIS 4+ injury probability versus BrIC based on MPS, the risk curve is shown in Figure 2.14.

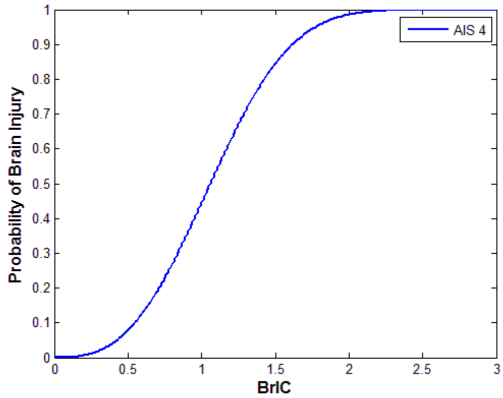

Figure 2.14: AIS 4 risk curve of BrIC based on MPS [32].

The critical angular velocities to be used with the BrIC were based on Maximum Principal Strain [33] as provided by a head FE-model and are given in Table 2.3.

Table 2.3: Critical Angular velocities in x, y and z directions

Critical angular velocity constants	Critical angular velocity (rad/s)
$\boldsymbol{\omega_{xC}}$	66.30
$\boldsymbol{\omega_{yC}}$	53.80
$\boldsymbol{\omega_{zC}}$	41.50

For soft tissue injuries maximum principal strain (MPS) in the brain tissue is used to analyze the injuries to the brain.

3 Method

This master thesis includes an evaluation of pedestrian's lower leg and head injury in vehicle-to-pedestrian collisions via FE simulations using THUMS KTH model. The Euro NCAP sub-system tests serves as a reference. Moreover, this thesis includes a feasibility study on accident reconstruction through FE simulations.

A parameter study was carried out that varied several major factors known to influence the pedestrian kinematics and injury risk. The factors under consideration were the impact velocity, impact height and impact location along the vehicle lateral direction.

The simulations in this study were performed using LS-DYNA version mpp971s R5.1.2, revision 85274 with 96 Number of Central Processing Units (NCPU's). All the data was filtered using Channel Frequency Class (CFC) 60 filter. The windscreen model used for the vehicle has an element thickness of 5.45mm and the deformation of it is controlled by the integration points defined for the part of the windscreen model. The vehicle FE-model used for analysis is an old small passenger model from Volvo.

The FE models used in this thesis were:

- THUMS KTH model
- Small PV model
- Flex-PLI GTR version 2.0 model
- Adult headform impactor model provided by Volvo Car Corporation.

3.1 Positioning of THUMS

The THUMS KTH model (hereinafter referred to as THUMS) has its initial stance with arms and left leg positioned anterior to the torso while the right leg posterior (Figure 3.1).

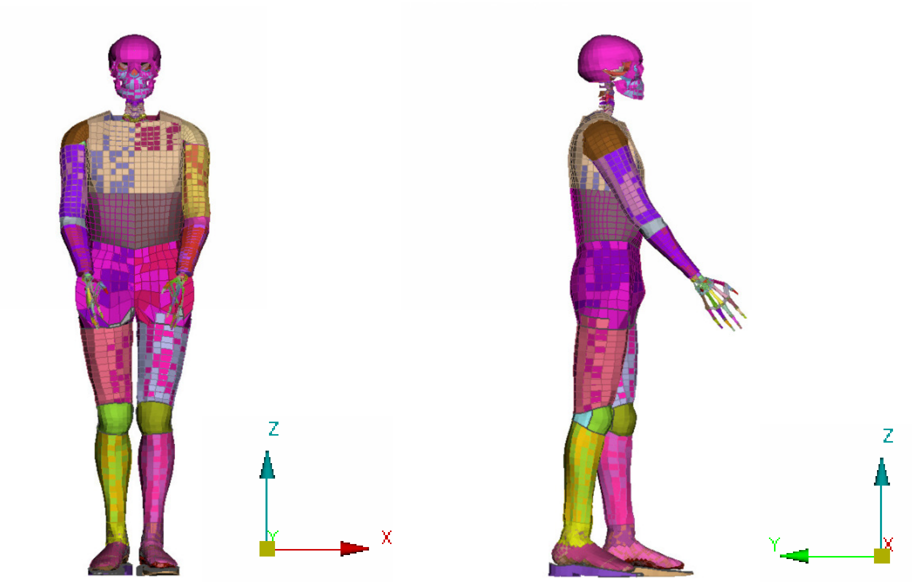

Figure 3.1: The front (left) and side (right) view of THUMS initial stance in global coordinate system

However, such stance is undesired as it is not representing any phase in a normal walking gait which is the most common posture in a pedestrian crash scenario [2]. A Matlab script named the Approximate Natural Movement Curve (ANMC), provided by Morén et al.[34], was utilized for moving the THUMS extremities. The final posture of the THUMS represent a stance in a normal walking gait. Due to the variation of pedestrian's step size, walking gesture as well as the phase to choose in a gait cycle, it is difficult to generalize. Therefore, European Union (EU) established the project IMVITER whose aim is to standardize regulations for virtual safety tests [35]. In this study, the desired walking stance is based on the end angle of the limbs as proposed by IMVITER, although this methods desirability is still under discussion [36]. Due to the difficulty of validating the head and neck movement, these body regions remained in their initial positions and changed to rigid while moving the extremities. A summary of initial and end position of extremities is shown in Table 3.1. The angles are about Y-Z plane of the global coordinate system (Same as provided in Figure 3.1). A positive value represents the extremities were anterior to the THUMS thorax and a negative value means a posterior position.

Table 3.1: Extremities' bone length and initial/ end angle.

Extremities		Length (mm)	Initial angle (degrees)	End Angle (degrees)
Upper arm	Left	283.4	21	5
	Right	283.4	21	– 30
Lower arm	Left	266.99	16.8	15
	Right	266.99	13	10
Upper leg	Left	434	2.9	– 7
	Right	434	– 7.1	13
Lower leg	Left	357.2	– 8.8	– 12
	Right	357.2	12.64	10

Finally, the feet were positioned using a procedure proposed by Ruth Paas, Chalmers. This modification was made to achieve a contact between the THUMS model and the ground.

Figure 3.2 below is the desired walking stance of THUMS after following the described procedure. Such posture will be the experiment posture of THUMS for all the simulations displayed in this thesis report. As can be seen, the THUMS now has a posture with left leg and right arm positioned posterior while right leg and left arm positioned anterior to the torso.

Figure 3.2: Walking Stance in global coordinate system

3.2 Impactor-to-vehicle simulations with comparison of THUMS

Legform simulations were performed by a Flex-PLI impactor model against the front-end of a FE vehicle model. An adult headform impactor model was also made to impact the windshield and bonnet. These simulations were performed for comparing the THUMS kinematics and injury risk under similar conditions. As the impacted leg of THUMS was positioned in walking gait, simulations were carried out where the legform impactor model was placed accordingly.

3.2.1 Legform simulations

The first series of legform-to-vehicle simulations was aimed at reproducing the required NCAP tests. The vehicle model was stationary and the impactor model was made to hit the vehicle with a velocity of 11.1 m/s (Figure 3.3). A gravitational force of 9.81m/s^2 was included in the simulations. Thus the distance between the impactor and the vehicle was calculated and selected when considering the falling distance of the legform. The default gap between the legform and the ground was 75 mm.

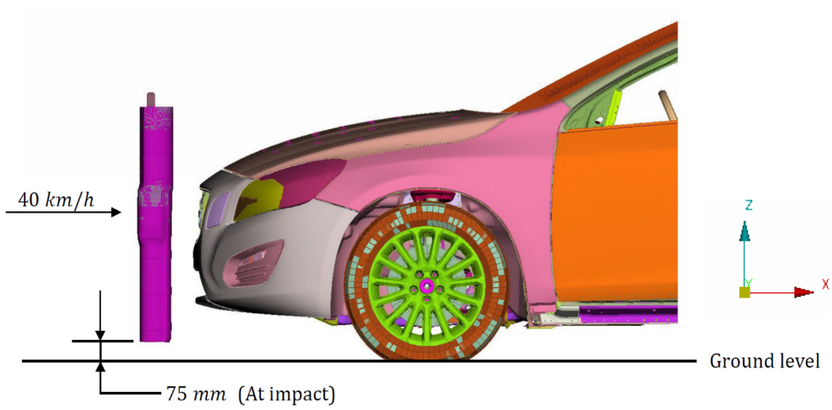

Figure 3.3: Legform-to-vehicle simulation test scenario (75mm above ground level)

For matching with the vertical position of the THUMS model in a walking stance, another scenario of legform-to-vehicle crash simulations was made according to knee position in global Z-axis (hereinafter referred to as walking position). A comparison between the THUMS lower extremity on the impact side with the respective Flex-PLI position is shown in Figure 3.4.

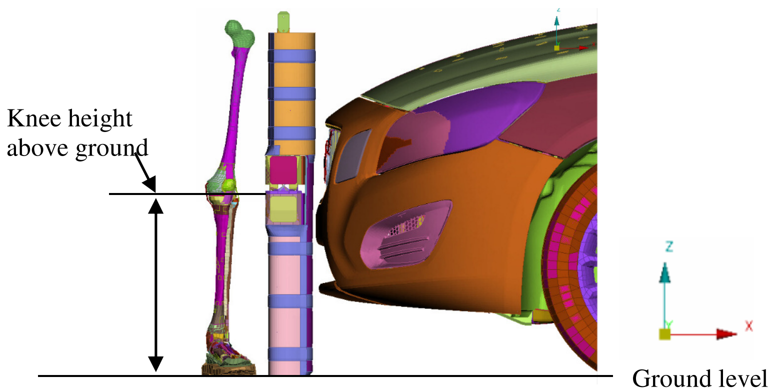

Figure 3.4 A comparison between the knee position of a THUMS model and a Flex-PLI placed accordingly

Moreover, several impact points on the energy absorber of bumper were selected, the positions are to be discussed in the section 3.3.

Euro NCAP pedestrian protocol suggests several measurements to be captured during testing, as shown in the Table 3.2.

Table 3.2: Flex-PLI legform impactor instrumentation and measurements

Location	Measurement
Tibia Bending	Tibia -1 Tibia -2 Tibia -3 Tibia -4
Knee Elongation	Medial collateral ligament (MCL) Anterior cruciate ligament (ACL) Posterior cruciate ligament(PCL)
Tibia	Acceleration (optional)

Tibia Bending Moment of Tibia-1, Tibia-2, Tibia-3 and Knee elongation of MCL, ACL, and PCL were measured in the simulations and compared with the THUMS model. In the Flex-PLI model, ligaments were presented as discrete springs, and tibia bending moments were calculated from the cross-sections defined on the tibia bone (Figure 3.5).

As of now there is no risk curve for predicting knee ligament injury. Although, the estimated thresholds of MCL, ACL and PCL elongation for Flex-PLI by Oliver et al. [37] will be considered for monitoring purpose. Such value indicates a 50% of injury risk. As presented, the MCL elongation threshold has a range from 16 mm to 23 mm while the ACL/PCL are suggested to have a limitation of 12.7 mm. The presented performance limitations were calibrated with 50th percentile male PMHS knee shearing results provided by the Flex-PLI evaluation group.

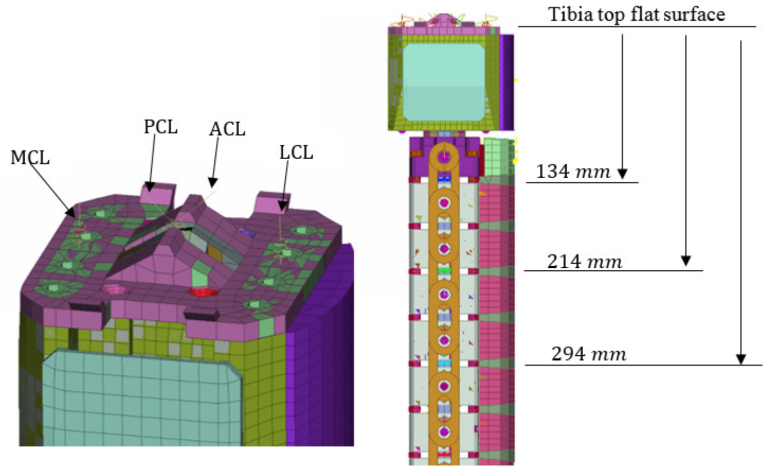

Figure 3.5: MCL, PCL, ACL, LCL in the knee area and the cross section selection (from top to bottom are Tibia -1, Tibia -2, and Tibia -3) in a Flex-PLI FE model

3.2.2 Headform simulations

In this study only adult headform impactor simulations were performed and these served as a reference. The adult head model was made to impact the vehicle at 65° to the ground reference level with a velocity of 11.1 m/s (Figure 3.6). Similar test setup is used in Euro NCAP tests.

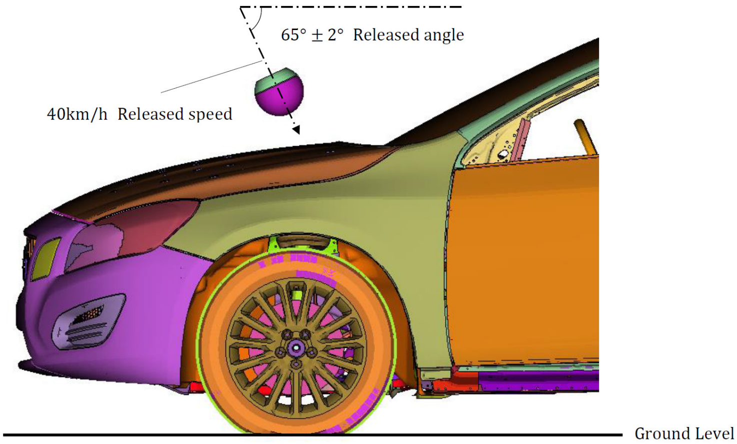

Figure 3.6: An example of adult headform simulation released at the grid point A.0.7

Due to time and resource capacity of the project, a limited number of headform simulations were carried out, instead of simulating on each grid point within the adult headform test zone. The chosen impact points were located onto the vehicle bonnet top, windscreen and the rigid fringe, the area around the wiper region, between bonnet and windshield.

The physical headform impactor consists of skin, sphere, accelerometer mount, and an end plate. The same components can be found in the FE model used in the computational simulation as well (Figure 3.7).

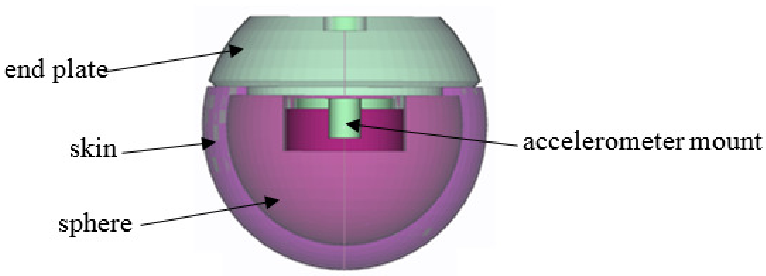

Figure 3.7: Headform impactor FE model

The measurement criteria required by Euro NCAP is HIC_{15} value on each grid points, which can also be coloured as shown below:

$$\begin{aligned} HIC_{15} < 650 &\quad = Green \\ 650 \leq HIC_{15} < 1000 &\quad = Yellow \\ 1000 \leq HIC_{15} < 1350 &\quad = Orange \\ 1350 \leq HIC_{15} < 1700 &\quad = Brown \\ 1700 \leq HIC_{15} &\quad = Red \end{aligned}$$

3.3 Vehicle-to-THUMS parameter study

The vehicle-to-THUMS parameter study includes simulations using THUMS with the rigid head model and the THUMS using the advanced head and neck model from KTH. The simulations were carried out at different impact velocities, vehicle heights and pedestrian impact locations. 36 simulations were carried out for each THUMS KTH model and a complete simulation matrix can be referred to Appendix 8.1.

Three vehicle velocities at 25km/h, 40km/h and 50km/h were simulated to analyse the effect of different vehicle velocities on the injuries sustained to pedestrian. The impact locations were varied by moving THUMS in the y-axis along the vehicle and the different vehicle heights used for this study has been referred from Morén et. al. [34]. Vehicle height was varied by moving the vehicle along z-axis. *Table 3.3* gives the different vehicle BLE heights and corresponding vehicle category accordingly.

Table 3.3: Scaling of vehicle according to BLE height above ground

Vehicle height	Vehicle category
694mm	Small PV
768mm	Large PV
877mm	Small SUV
988mm	Large SUV

Knee ligaments and tibia injuries were studied in THUMS. The modelling of ligament behaviour was achieved by defining the ligament material with material type 19, a strain rate dependent material which will cause failure and element deletion if the effective strain rate researched the predefined stress-strain load curve. To analyse the injuries to ligaments,

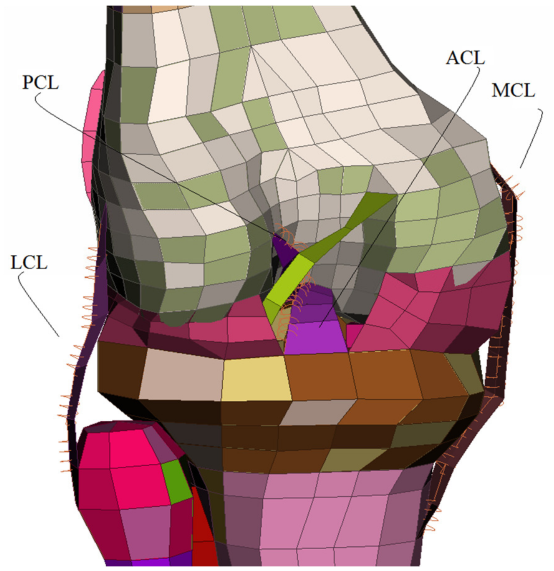

Figure 3.8: Weak springs attached to the ligaments of knee of the THUMS (posterior view)

a series of weak springs were attached to the corresponding knee ligaments in THUMS model. The three ligament injuries analysed were for MCL, PCL and ACL. The spring arrangement is shown in figure 3.8.

However, the ability of THUMS predicting knee injury is questioned by several researchers and studies, the material property and definition of ligament needs to be re-examined [38] [39]. In the computational simulations done in this report, the shell elements were mostly highly distorted when exposed to impact, and the behaviour was also undesired as it can hardly be representative as human knee ligaments. Due to such reason, further study in this thesis work only present the result of ligament injury but not to be analysed.

For analysing injuries sustained to tibia, bending moments of the tibia bone have been used as a measure. In the THUMS FE model, tibia cortical bone is represented by shell elements and the tibia spongy bone is represented by solid elements. The FE behaviour were achieved by two integrated materials defined for both shell and solid elements, which are the Material Type 105 and Material Type 24. The element failure and deletion of these two material were caused by plastic strain reaching the defined values. Such value for the shell elements representing the cortical bone is set to be 0.06, while the solid elements are having a value of 0.33 to achieve a more elastoplastic behaviour of the spongy bones.

To obtain the bending moments from LS-DYNA for the tibia bone, a series of cross-sections using shell and solid elements were defined for the THUMS model. A detailed set-up of the cross-sections for the left leg of the THUMS model is shown in Figure 3.9.

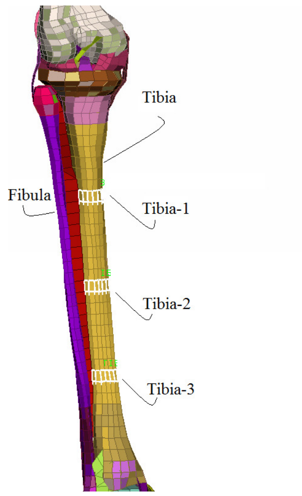

Figure 3.9: Tibia cross sections in the THUMS

Three cross-sections were defined; Tibia-1 for upper tibia bending moment, Tibia-2 for mid-upper tibia bending moment and Tibia-3 for mid-lower tibia bending moment (Figure 3.9). These cross-sections were selected based on the location of the cross-sections on Flex-PLI legform impactor model.

For injury analysis to the head, a node has been defined in the THUMS model at the centre of gravity of the head which is attached to a rigid part of skull. Accelerations used to calculate different injury criteria for head were obtained from this node output.

The impact location of THUMS is selected at five different points in the y-direction along the energy absorber. These impact points are P1 (y=-400mm), P2 (y=-300mm), P3 (y=0mm), P4 (y=200mm) and P5 (y=530mm). The negative sign represents that the impact location is to the left side of the vehicle midline and the positive sign represents the right side of the vehicle midline. The impact point P3 is in the midline of the vehicle and the other impact points are offset from it in the y-axis. Impact points P2, P3 and P4 were used for comparison between impactor-to-vehicle simulation and vehicle-to-THUMS simulation results. While the impact points P1, P3 and P5 were only used for the parameter

Figure 3.10: Impact points on the front energy absorber for pedestrian position in front of the vehicle, along the y-axis

study of vehicle-to-pedestrian collisions. The reason for using this impact points for parameter study is that for impact point P5, the impact of lower leg takes place at the edge of the energy absorber, P1 near to the edge and P3 in midline. Thus these cases were identified as interesting to study as analysis of the injuries sustained to the lower leg of pedestrian even when the impact takes place at the edge of the energy absorber could be carried out and also using such wider offsets would help analyse the injuries sustained to the head at wide range of impacts points along the WAD on bonnet and windshield of the vehicle. As can be seen, the impact point P5 is on the edge of the energy absorber.

3.4 Accident reconstructions

Accident reconstructions were carried out based on V_PAD accident database and using same version of LS-DYNA. . The source of data is insurance company Volvia, police report and questions asked to victim or victim's personal contacts [6]. The database contains information like the impact speed, traffic environment, pedestrian impact points, car damage and injuries sustained. Injuries are coded based on AIS. Using information about the pedestrian before, during and after a collision it is possible to reconstruct such a real-life accident database case into computer simulations.

The scenario setup was performed using the pre-processor ANSA Ver 15.1.3. Using the variables in the accident database, the position of pedestrian before collision could be estimated. Data regarding kinematics of pedestrian and injuries sustained after the collision could also be extracted from the database.

A total of two vehicle-to-pedestrian accidents were analysed regarding injuries sustained to the pedestrian using accident reconstructions. Pedestrian details and reconstruction data details are presented in Table 3.4 and Table 3.5 respectively.

Table 3.4: Accident database summary of pedestrian information

Pedestrian ID	Gender	Age	Stance	Injury type	AIS
1	Male	27	Walking	Concussion	3
2	Male	79	Running	Fracture	2

Table 3.5: Accident database summary of reconstruction data

ID	Vehicle model	Vehicle type	Vehicle Speed	Impact location
1	S80	Large PV	50km/h	On windshield
2	V70	Large PV	50km/h	Y = -15

The two cases and the corresponding scenario are discussed as follows:

Case 1: On a dark and rainy day, a vehicle driver is driving at 50km/h. A 27 years old male appears walking from right side of the vehicle, the collision happens and the pedestrian head impacts the windshield of the vehicle.

The vehicle is identified as a large passenger vehicle. The alcohol level of pedestrian is not known and the pedestrian is transported to the hospital in an ambulance after the collision. The MAIS level identified is 3. The pedestrian suffers from brain concussion injury which corresponds to an AIS 3 injury level.

The vehicle-to-pedestrian collision setup for case 1 is shown in figure 3.11.

Figure 3.11: Reconstruction case 1 vehicle-to-pedestrian collision setup

Case 2: On a dark day with poor street lighting, a vehicle driver is driving on a city street road at 50km/h, just after a three-way intersection, a 79 years old male pedestrian appears running and is hit by the vehicle. During collision, the pedestrian is thrown on bonnet and windshield of the vehicle and sustains fracture of skull, shin, ribs and pelvis.

The vehicle is identified as a large passenger vehicle. The pedestrian is identified as drunk and is transported to the hospital in an ambulance after the collision. The MAIS level is identified as 3. The pedestrian suffers from a skull fracture which corresponds to AIS 2 injury level.

The vehicle-to-pedestrian collision setup for reconstruction case 2 is shown in figure 3.12.

Figure 3.12: Reconstruction case 2 vehicle-to-pedestrian collision setup

4 Results

In this chapter, the results from the impactor-to-vehicle simulations are compared to those of the THUMS and also vehicle-to-THUMS parameter study results are presented.

4.1 Impactor-to-vehicle simulations with comparison of THUMS

This section presents the results from the simulations of impactors striking the vehicle. The impactor data are also compared with those obtained in simulations using the THUMS model for similar test conditions and the same injury criteria.

4.1.1 Lower leg injuries

For comparison between the leg impactor and the THUMS results, a small passenger vehicle with impact points P2, P3, P4 and impact velocity 40km/h has been used. Figure 4.1 shows the kinematic behaviour of THUMS and Flex-PLI legform impactor in the simulated collision at impact point P3.

Figure 4.1: Kinematic behaviour of THUMS impact leg and Flex-PLI collision with vehicle, THUMS impact side leg (left), Flex-PLI (75mm above ground, middle), Flex-PLI (walking position, right)

The results of ligament injury on Flex-PLI FE model impacting the pre-defined points P2, P3 and P4 are studied with two different vertical positions. Complete Flex-PLI ligament elongation curve can be found in Appendix 8.2.1 which is normalized by taking the MCL elongation of THUMS model at P3 as default. Comparing between these two Flex-PLI height sets, 75mm above the ground level has higher peak values of MCL elongation than the walking position. The maximum MCL elongation occurs at around 40ms when Flex-PLI is positioned 75mm above ground and around 25ms at walking position. The knee ligament (MCL, ACL and PCL) elongation curves of THUMS model placed at the same impact points as Flex-PLI considered above is shown in Figure 4.2.

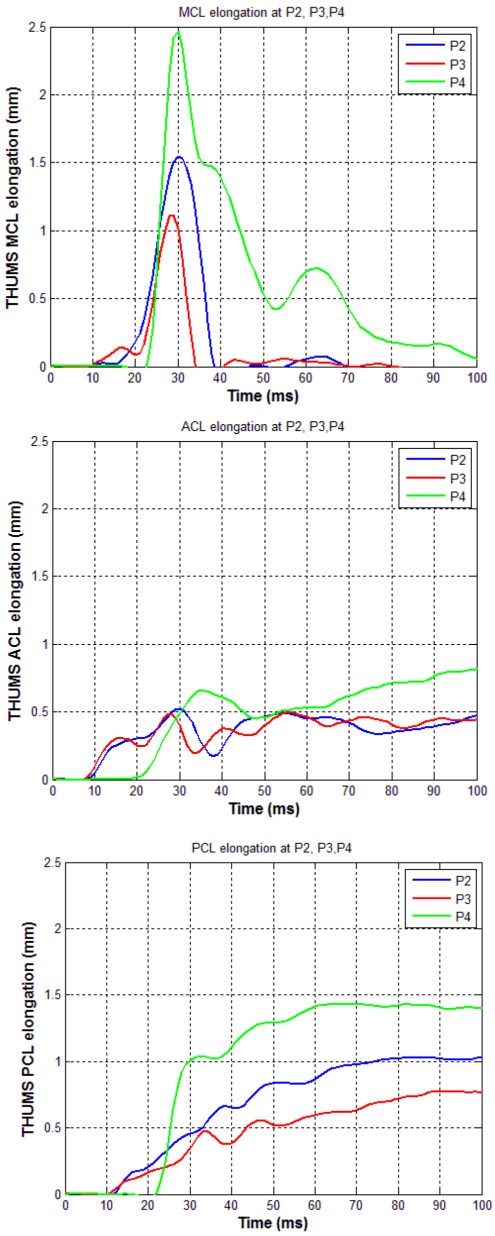

Figure 4.2: MCL (top left), ACL (top right), PCL (bottom) elongation curve of THUMS model at P2, P3, P4

For the THUMS model, the impact point P4 shows the highest maximum elongation values for all three ligaments. The other two impact points, P2 and P3, have similar curve shape. While P3 provided the lowest maximum elongations.

Table 4.1 below presents all the maximum ligament elongations values of THUMS model, Flex-PLI positioned 75mm above the ground and Flex-PLI positioned according to the walking stance of THUMS model.

Table 4.1: Maximum ligament elongations of Flex-PLI with two different vertical position and THUMS model of walking stance

MCL elongation	**P2**	**P3**	**P4**
THUMS	1.4	1.0 (N)	2.3
Flex – PLI (75mm)	12.8	8.9	9.5
Flex - PLI(walking position)	7.5	3.1	3.5
ACL elongation	**P2**	**P3**	**P4**
THUMS	0.5	0.5	0.7
Flex – PLI (75mm)	4.2	2.5	3.0
Flex - PLI(walking position)	2.4	1.7	1.5
PCL elongation	**P2**	**P3**	**P4**
THUMS	0.9	0.7	1.3
Flex – PLI (75mm)	4.3	3.1	3.4
Flex - PLI(walking position)	3.8	2.4	1.5

The comparison of maximum tibia bending moments for the three different tibia cross-sections for impact points P2, P3 and P4, can be seen in Figure 4.3. Two positions of Flex-PLI were included in the comparison.

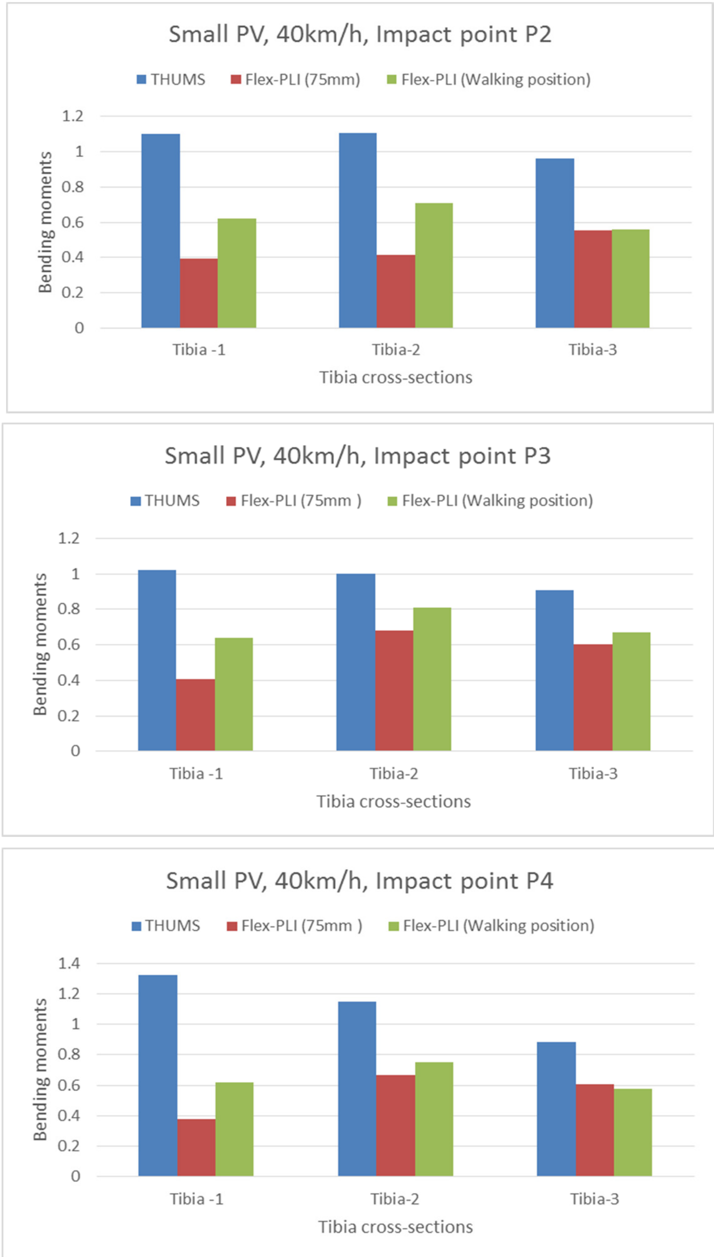

Figure 4.3: Tibia bending moment comparison between THUMS and Flex-PLI at impact point P2 (top), P3 (middle) and P4 (bottom)

Overall, the Flex-PLI impactor had lower bending moments than THUMS for all the impact points and tibia cross-sections. The resultant bending moment curve comparison between THUMS and Flex-PLI for different tibia cross-sections can be found in Appendix 8.3.1.

4.1.2 Head injuries

A total of 6 cases were selected from simulation matrix (Appendix 8.1) based on different vehicle heights, vehicle velocities, head impact locations on the vehicle and the severity of head injury (Table 4.2). The data presented henceforth has been normalized by taking the case of Small PV, 40 km/h and impact point P3 as nominal load case.

Table 4.2: Summary of 6 cases for head injury comparison between THUMS and headform impactor

Case no.	Simulation number	Vehicle type	Vehicle impact velocity (km/h)	THUMS location along vehicle energy absorber	Head impact point
Case 1	2	Small PV	40	P3	H1
Case 2	13	Small PV	25	P1	H2
Case 3	1	Small PV	40	P1	H3
Case 4	17	Large PV	25	P3	H4
Case 5	28	Large PV	50	P1	H5
Case 6	6	Large PV	40	P5	H6

Figure 4.4 shows the vehicle with the six head impact locations. Since, small passenger vehicle was used to mimic different vehicle types, so the head impact locations for different vehicle types have been shown on the same vehicle surface.

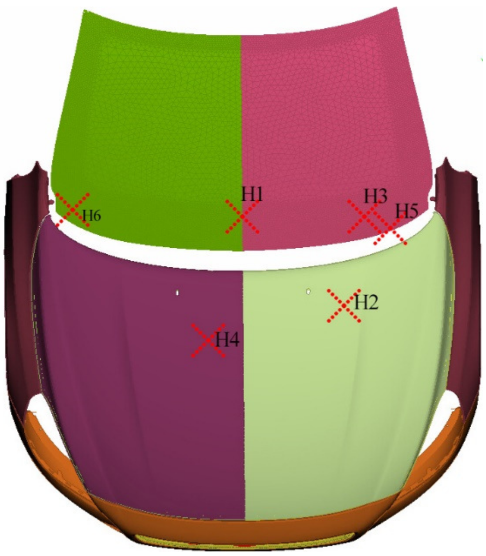

Figure 4.4: Head impact location for the 6 cases

The linear head acceleration comparison for THUMS (rigid head model) and headform impactor for the six cases are shown from figure 4.5 - figure 4.7.

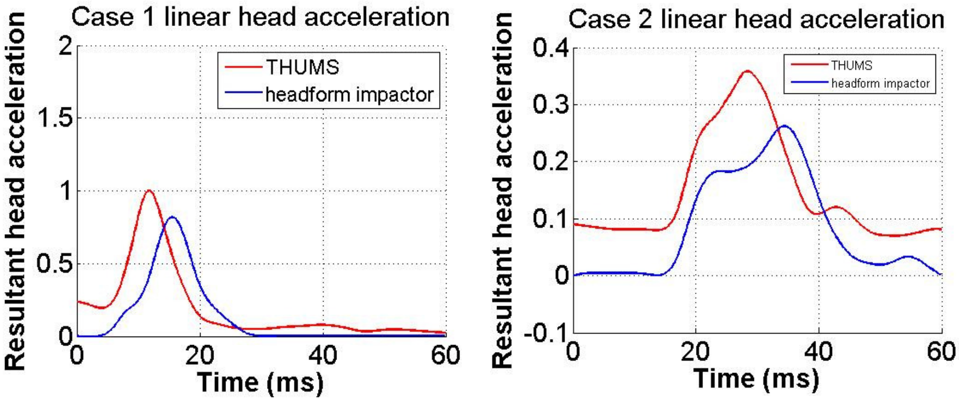

Figure 4.5: Case 1 (left) and Case 2 (right)

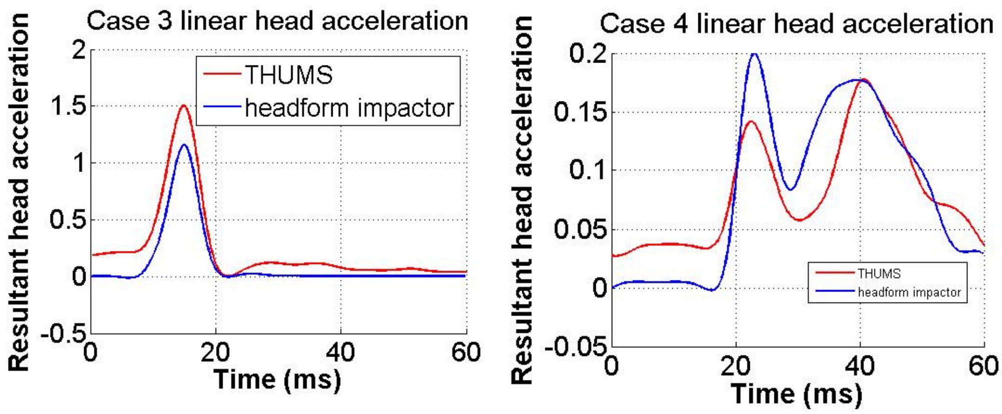

Figure 4.6: Case 3 (left) and Case 4 (right)

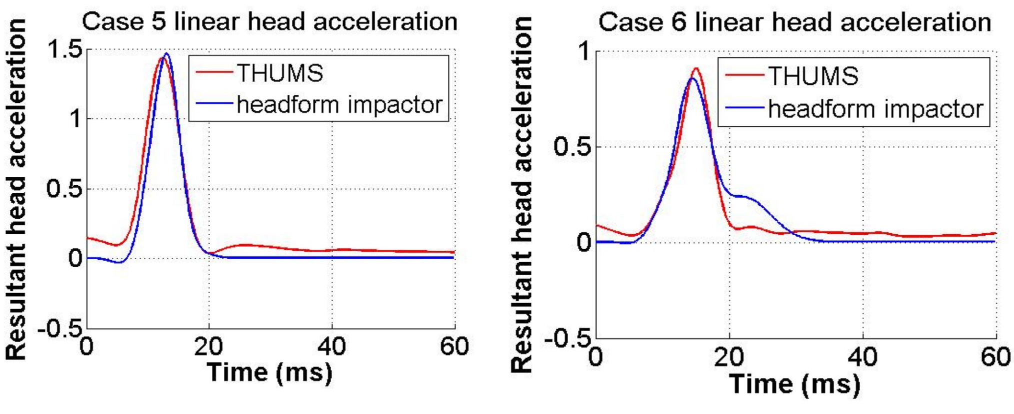

Figure 4.7: Case 5 (left) and Case 6 (right)

The curves have been overlaid by comparing the time at which there is significant increase in the acceleration value, removing the rest of the data which is not useful for comparison. As can be seen from the resultant head linear accelerations for the six different cases, THUMS and headform impactor shows a similar trend for the impact duration and have similar peak values at impact velocities of 40 and 50 km/h while there is some deviation at lower impact velocity of 25 km/h. For THUMS, the initial head acceleration level while impacting with vehicle is not zero because of the fact that the THUMS head is already in motion due to impact kinematics and thus this leads to the increase of initial head acceleration.

The maximum linear acceleration of head and the corresponding HIC_{15} values for THUMS and headform impactor for the six cases above are shown in table 4.3.

Table 4.3: Resultant head linear acceleration and HIC_{15} for the 6 cases

Case no.	Simulation number	Resultant head acceleration		Head Injury Criteria (HIC_{15})	
	THUMS	THUMS	Headform	THUMS	Headform
1	2	1 (N)	0.82	1(N)	0.64
2	13	0.32	0.26	0.17	0.08
3	1	1.50	1.16	2.33	1.05
4	17	0.18	0.20	0.03	0.035
5	28	1.44	1.47	2.20	1.90
6	6	0.91	0.85	0.58	0.59

Figure 4.8 shows the correlation analysis between THUMS and headform impactor for HIC_{15} values.

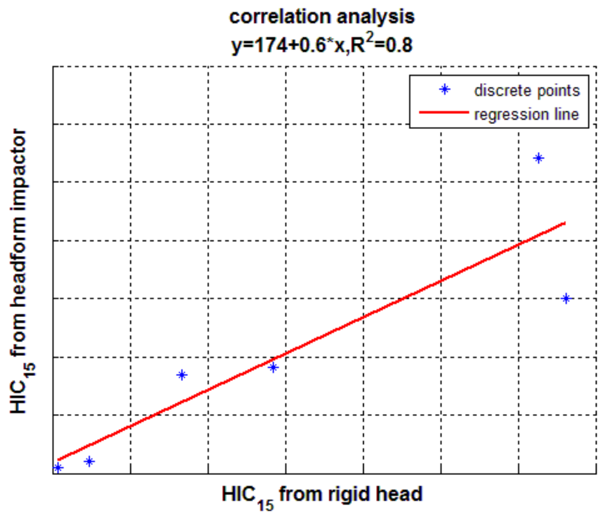

Figure 4.8: Correlation analysis of HIC_{15} between THUMS and headform impactor

For different vehicle heights, vehicle velocities and impact locations on vehicle, THUMS is able to produce the same trend and behaviour in terms of acceleration curve and impact duration. However, the peak values of acceleration is offset between the two models which leads to a relatively low correlation in HIC $_{15}$ prediction between the two models.

4.2 Vehicle-to-THUMS parameter study

For the parameter study THUMS with a walking stance was positioned in front of the vehicle with the impact side leg posterior to the body. An example of this setup for a small PV at impact point P3 can be seen in figure 4.9.

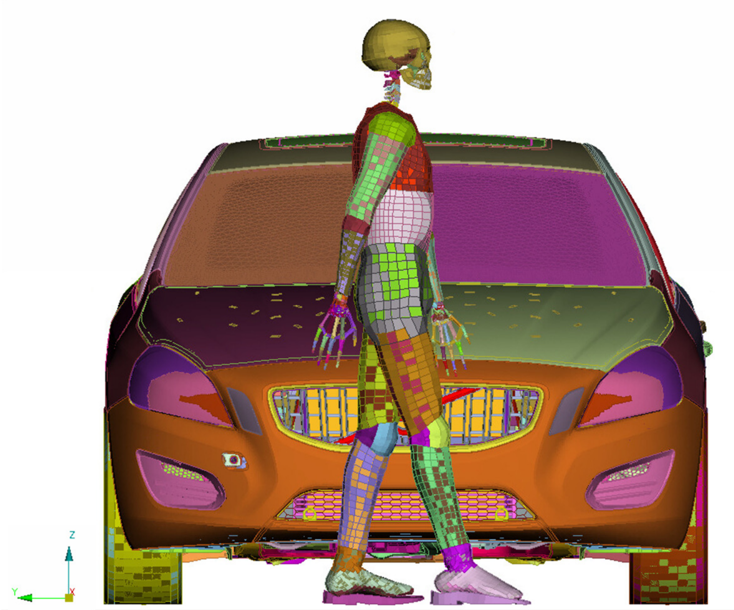

Figure 4.9: Vehicle-to-THUMS collision simulation setup

This parameter study includes an analysis of different vehicle heights, vehicle velocities and impact locations on the risk of injuries to lower leg and head. While studying lower leg injuries, only the small PV was used as a reference vehicle as different vehicle heights will result in different lower leg impact positions.

Figure 4.10 shows the vehicle-to-pedestrian interactions as predicted in the THUMS simulations for a small PV at 25km/h, 40km/h and 50km/h vehicle velocities and impact point P1.

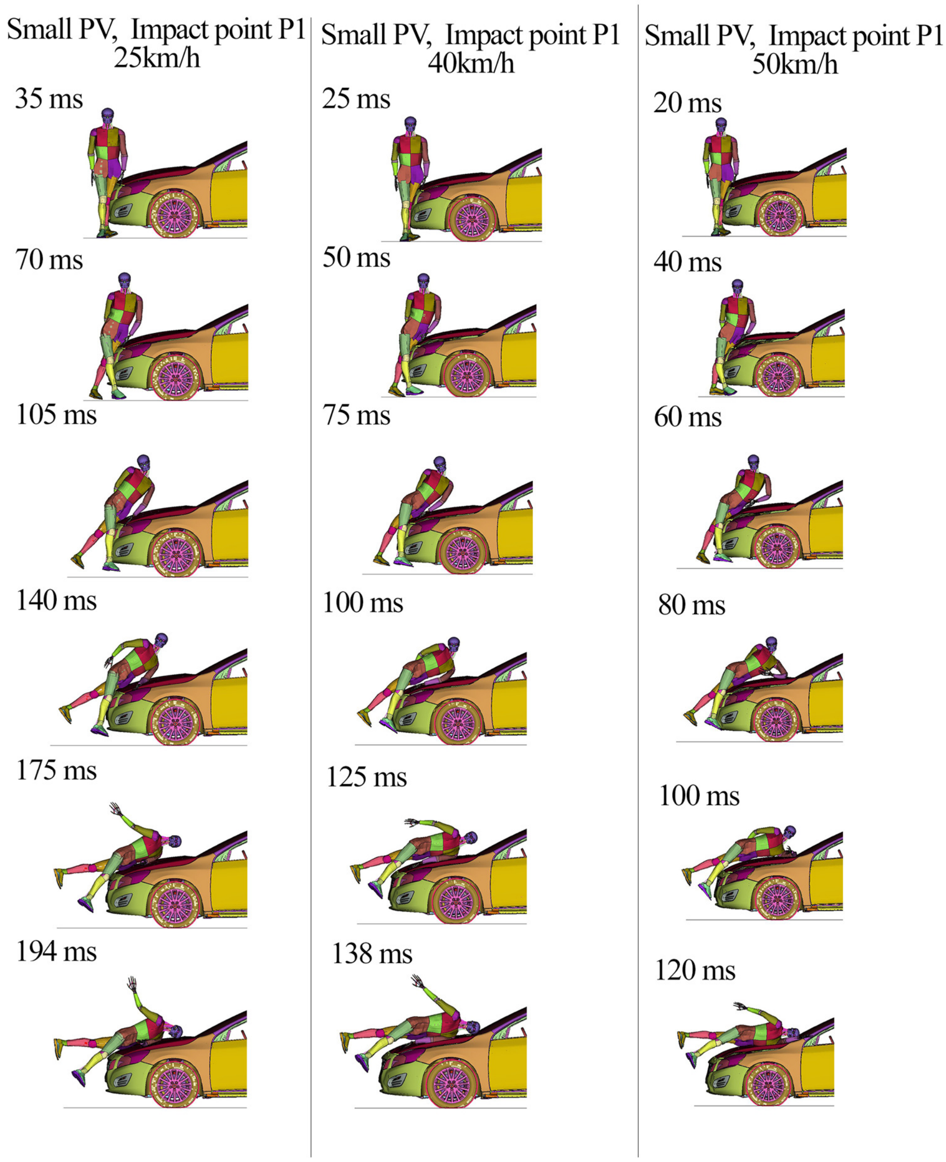

Figure 4.10: THUMS interaction with small PV when hit at P1 in 25km/h, 40km/h and 50km/h

4.2.1 Lower leg injuries

Appendix 8.2.2 shows ligament elongation comparison with variation of impact points P1, P3 and P5 at different velocities: 25km/h, 40km/h and 50km/h. The case of impact point P3 under 50 km/h was eliminated due to the deletion of elements on PCL, which was considered as a simulation failure.

The highest elongation value of MCL and ACL/PCL were obtained for P5 as compared to the other two locations with the exception of the case explained above. With the velocity increasing, the difference becomes more pronounced, especially for MCL elongations. Appendix 8.2.3 presents ligament elongation with variation of vehicle velocities of 25km/h, 40km/h and 50km/h at different impact points. The highest displacement values for each case always occurs at 50km/h. P1 and P5 display lower MCL stretch when the impact velocity decreases. For P3, however, the elongation of MCL is almost the same for the different velocities.

The tibia bending moments for different tibia cross-sections is listed in table 4.4 for different vehicle velocities and different impact points.

Table 4.4: Tibia bending moments for different vehicle velocities and different impact points for the different tibia cross-sections.

Vehicle speed (km/h)	Tibia-1			Tibai-2			Tibia-3		
	P1	P3	P5	P1	P3	P5	P1	P3	P5
25	1.23	1.15	0.96	1.06	1.06	0.58	0.79	0.83	0.29
40	1.33	1.03	1.20	1.21	1.00 (N)	0.73	0.99	0.90	0.40
50	1.55	1.09	1.00	1.27	0.99	0.67	1.00	0.97	0.66

Figure 4.11 shows the maximum tibia bending moments in the three tibia cross-sections for vehicle velocity 25 km/h at three positions.

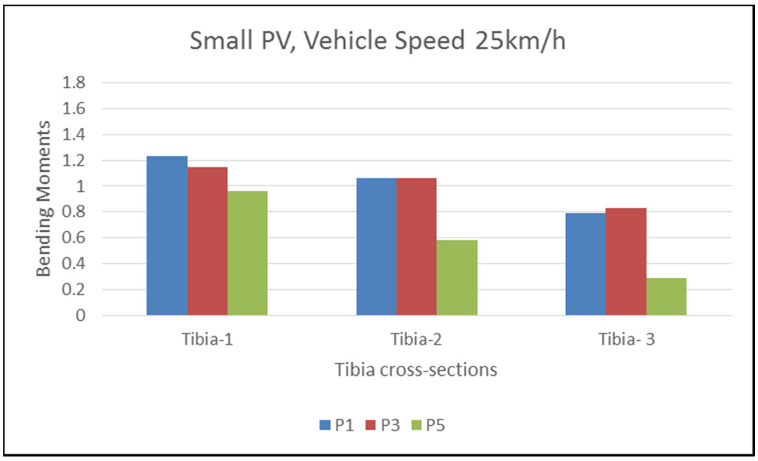

Figure 4.11: Maximum bending moment for small PV at different impact points at 25km/h

The overall trend shows that for different impact points, the maximum moment is for tibia-1 cross-section followed by tibia-2 and tibia-3. Impact point P5 which is on the edge of energy absorber has lower tibia bending moments than impact point P1 and P3 for all the tibia cross-sections. Impact point P1 which is near to the edge of the energy absorber has generally higher tibia bending moments than the other two impact points.

Figure 4.12 shows the stresses in the vehicle front components when the bending moment of tibia is at its maximum for impact point P1 and velocity 25 km/h.

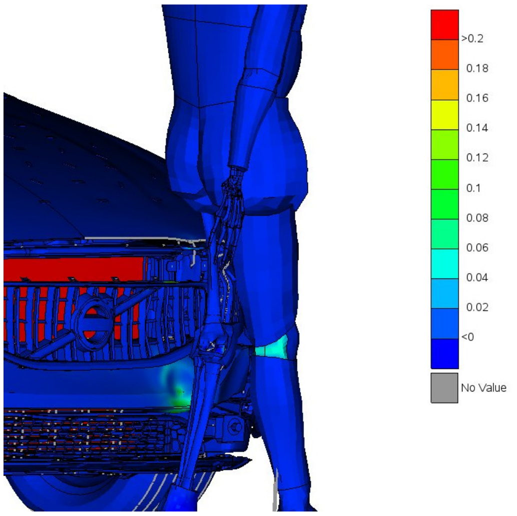

Figure 4.12: Fringe plot of stress in MPa for the vehicle front when THUMS was impacted at 25 km/h at impact point P1

For this case, the energy absorber of the vehicle has maximum contact area with the upper part of the tibia bone which is close to the tibia-1 cross-section.

Figure 4.13 shows the maximum tibia bending moments in the three tibia cross-sections for vehicle velocity 40km/h.

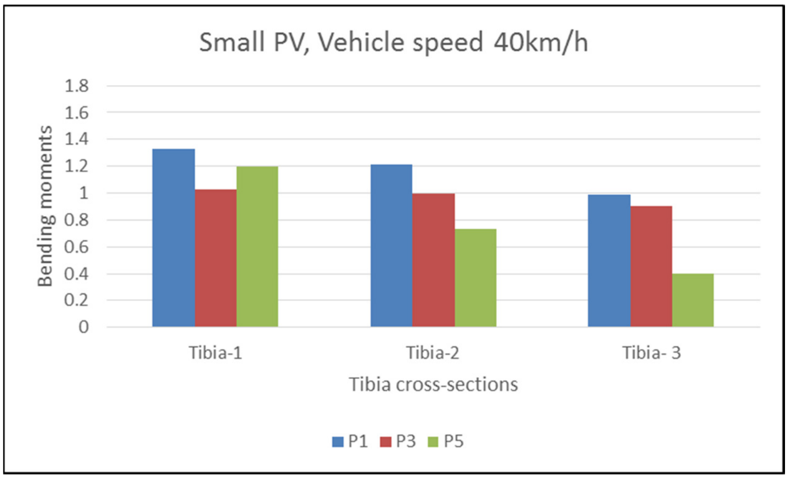

Figure 4.13: Maximum bending moment for small PV at different impact points at 40km/h

For all the impact points, tibia-1 experiences the maximum bending moment than the other two cross-sections. Impact point P1 has highest tibia bending moment for upper tibia cross-section i.e. tibia-1, impact point P3 has lowest tibia-1 bending moment.

Figure 4.14 shows the stresses in the vehicle front components when the bending moment of tibia is at its maximum for impact point P1 and velocity 40 km/h.

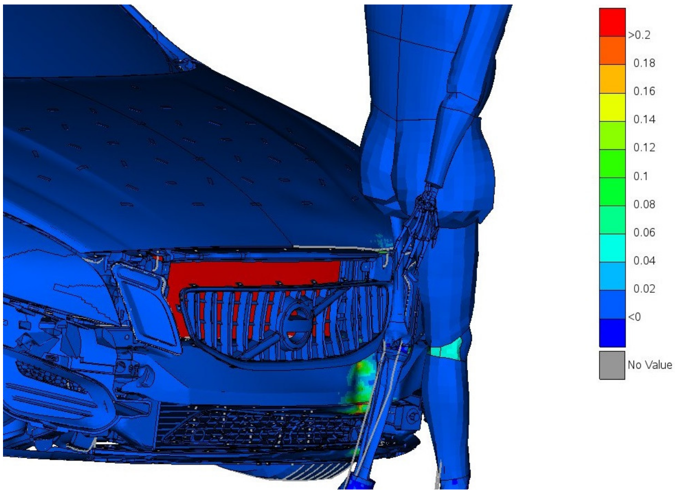

Figure 4.14: Fringe plot of stress in MPa for the vehicle front when THUMS was impacted at 40 km/h at impact point P1

As can be seen from figure 4.14, for this case the impact side lower leg comes into maximum contact with the edge of the energy absorber at the tibia-1 cross-section.

Figure 4.15 shows the maximum tibia bending moments in the three tibia cross-sections for vehicle velocity 50km/h.

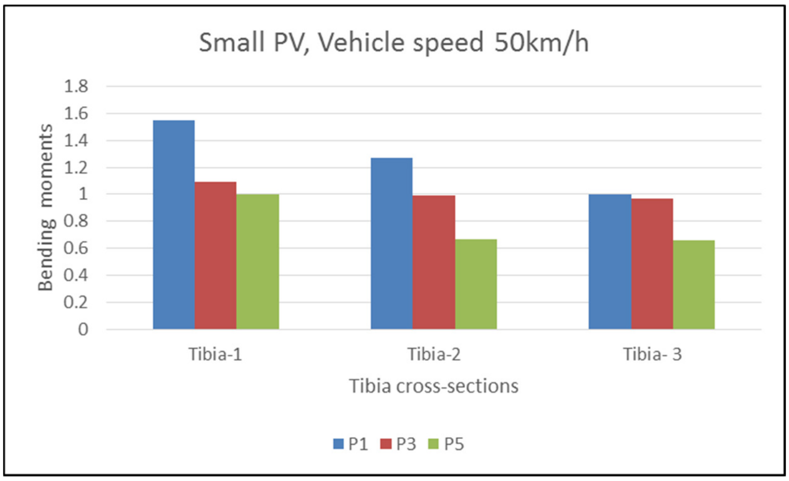

Figure 4.15: Maximum bending moment for small PV at different impact points at 50km/h

The maximum bending moments are seen for tibia-1 cross-section at impact point P1. The overall trend shows that tibia-1 bending moment is greater for all the impact points than the other two cross-section bending moments.

Figure 4.16 below shows the stresses on vehicle and impact location of leg for critical impact point P1.

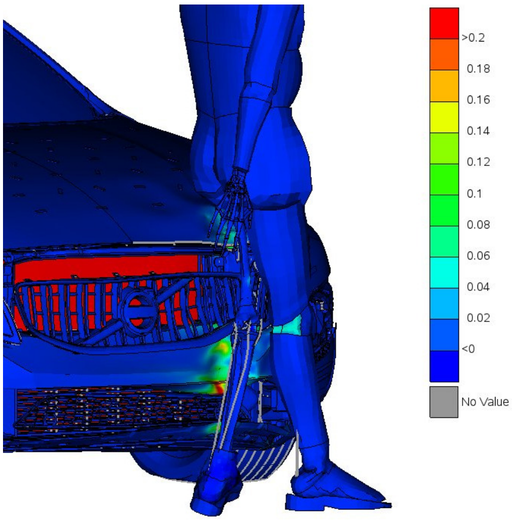

Figure 4.16: Fringe plot of stress in MPa for the vehicle front when THUMS was impacted at 50 km/h at impact point P1

In this case, the edge of the energy absorber has maximum contact with upper part of tibia bone (tibia-1 cross-section) at maximum tibia-1 bending moment.

Figure 4.17 shows the variation of maximum tibia bending moments for different impact points for the small passenger vehicle with variation of vehicle velocities.

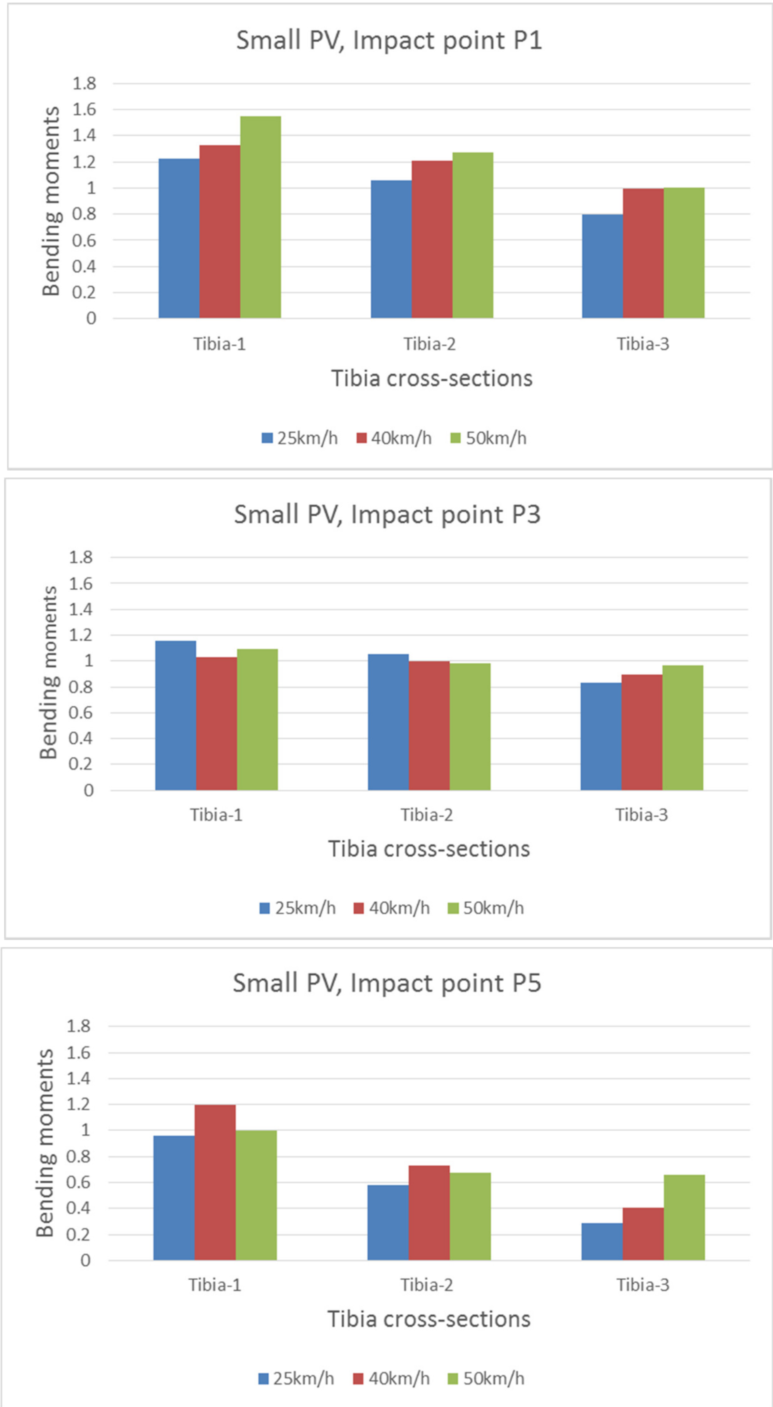

Figure 4.17: Maximum bending moment for small PV for different vehicle velocities for impact point P1 (top), impact point P3 (middle) and impact point P5 (bottom)

The overall trend shows that tibia-1 bending moments are high than other two cross-section bending moments. For impact point P1, the tibia-bending moment is maximum for tibia-1 followed by tibia-2 and tibia-3. As vehicle velocity increases, the bending deformation increases. For impact point P3, which is in the midline of the energy absorber, tibia-1 cross-section bending moment is higher for 25km/h and lower for 40km/h and 50km/h. For impact point P5, the highest bending deformation is observed at tibia-1 for impact point 40km/h. This impact point is on the edge of energy absorber, the tibia cross-sections have minimal contact with the vehicle front with maximum contact being with the upper part of lower leg.

Figure 4.18 and 4.19 shows the femur behavior at different vehicle velocities for impact point P3 and P5 respectively.

Figure 4.18: Fracture of femur at maximum tibia bending moment at 25km/h (top left), 40km/h (top right) and 50km/h (bottom) for impact point P3

Figure 4.19: Fracture of femur at maximum tibia bending moment at 25km/h (top left), 40km/h (top right) and 50km/h (bottom) for impact point P5

For impact point P3, the femur did not fracture at 25km/h but fractured at 40km/h and 50km/h. For impact point P5, the femur fractured for 50km/h vehicle velocity at maximum tibia bending moment.

The detailed bending moment curves for different cases and tibia cross-sections can be found in Appendix 8.3.2 and Appendix 8.3.3.

4.2.2 Head injuries

In the following analyses of head injuries different vehicle heights, impact velocities and impact locations have been considered.

Appendix 8.4.1 shows the resultant head impact velocity and resultant head linear acceleration for different vehicle heights and impact points. Simulation number 14, 34, 35, 40, 43 and 72 (appendix 8.1) resulted in error due to abnormal increase in hourglass energy for some of the elements. Effort was not made to solve the issues as changing some element properties in THUMS model might have changed its behaviour. So, results of these cases are not presented henceforth. The data presented henceforth is normalized by taking the load case of Small PV, 40km/h and impact point P3 as nominal.

For the study, two head models have been used. The reason for using two head models is that the injury criteria HIC and BrIC and related risk functions are developed for the dummy head which does not consist of a model of a flexible brain [30] [40]. And, for analysing the injuries sustained to the brain like maximum principal strain in the brain tissue, the advanced KTH head and neck model with brain is used. Further, the effective mass of both the head models is different which results in different linear accelerations of head and the HIC measured.

The displacement curve of head from both these models for the small passenger vehicle at 40km/h and impact point P3 is shown in figure 4.20.

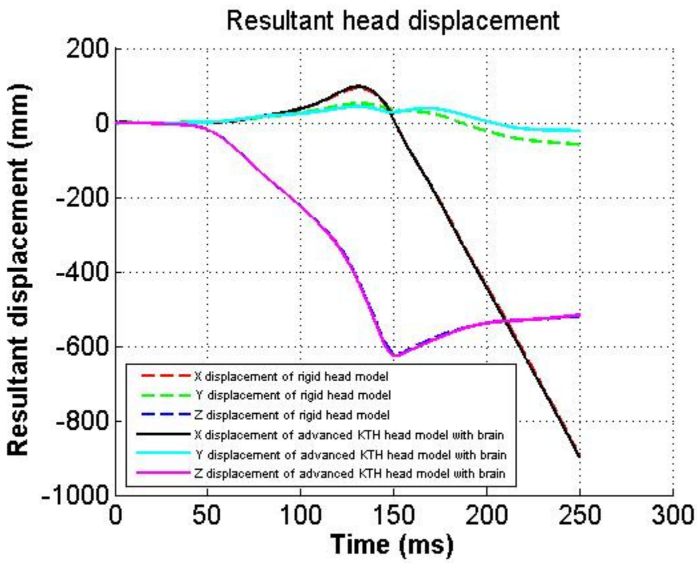

Figure 4.20: Resultant head displacement in x, y and z direction comparison for rigid head model and advanced KTH head model with brain

As seen from the figure, the head displacement of THUMS model with rigid head model is a close representative of the model with advanced KTH head and neck model with brain.

So, it can be assumed that simulations with these two head models will result in head impact at similar locations on vehicle.

For all the cases considered, it was observed that for a particular vehicle model, the head impact velocities depended on interaction with vehicle front and head linear accelerations increased with increasing vehicle velocities and increasing stiffness at the point of impact. For different vehicle heights, 25km/h vehicle velocity produced low head linear accelerations whereas 50km/h produced high head linear accelerations. The magnitude of linear head accelerations varied and it depended on 1) Impact location of head on vehicle (either bonnet or windshield) and 2) Pedestrian impact point with respect to bumper beam as discussed in section 3.3. The region of impact on windshield produced lower head linear accelerations because of more deformation whereas due to the presence of dashboard members beneath the windshield, such impact points produced high linear head accelerations.

Table 4.5 lists the maximum value of resultant head impact velocities and head linear accelerations for all the cases using THUMS KTH model with rigid head.

Table 4.5: Maximum of resultant head linear accelerations and resultant head impact velocities for different impact points and vehicle velocities

Type of vehicle	Vehicle speed (km/h)	Resultant head impact velocity			Resultant head acceleration		
Vehicle impact points →		P1	P3	P5	P1	P3	P5
Small PV	25	0.77	error	0.57	0.36	error	0.25
Small PV	40	1.02	1(N)	0.87	1.51	1(N)	0.35
Small PV	50	1	1.13	1.04	0.64	1.26	0.57
Large PV	25	0.66	0.62	0.55	0.23	0.18	0.24
Large PV	40	0.94	0.98	0.83	0.50	0.58	0.91
Large PV	50	1.02	1.21	0.98	1.44	1.12	0.72
Small SUV	25	0.66	0.70	0.57	0.23	0.25	0.24
Small SUV	40	0.98	1.02	0.79	1.10	0.97	0.69
Small SUV	50	1.19	1.26	1	1.17	1.01	1.57
Large SUV	25	0.70	0.72	0.64	0.26	0.23	0.23
Large SUV	40	1.09	1.06	0.91	0.94	0.95	1.12
Large SUV	50	error	error	1.25	Error	error	1.11

Table 4.6 lists the HIC_{15} calculated for different vehicle heights, vehicle velocities and impact points with the rigid head model.

Table 4.6: HIC_{15} for different vehicle heights, vehicle velocities and impact points

Type of vehicle	Vehicle speed (km/h)	HIC_{15}		
Vehicle impact points →		P1	P3	P5
Small PV	25	0.17	error	0.06
Small PV	40	2.33	1.00 (N)	0.19
Small PV	50	0.79	1.74	0.71
Large PV	25	0.05	0.03	0.05
Large PV	40	0.36	0.41	0.58
Large PV	50	2.20	1.43	0.56
Small SUV	25	0.04	0.06	0.05
Small SUV	40	1.18	1.02	0.60
Small SUV	50	1.76	1.39	2.45
Large SUV	25	0.09	0.08	0.06
Large SUV	40	1.31	1.32	1.31
Large SUV	50	error	error	2.16

For all the cases, a vehicle velocity of 25km/h shows a low risk of head injury. For a velocity of 50km/h, the risk of AIS3+ head injury risk is high except for the small PV at the P1 and P5 impact positions and for Large PV at the P5 impact position.

The head impact locations for different vehicle heights and pedestrian impact points for vehicle velocity of 25km/h, 40km/h and 50km/h are shown from figure 4.21 – 4.23.

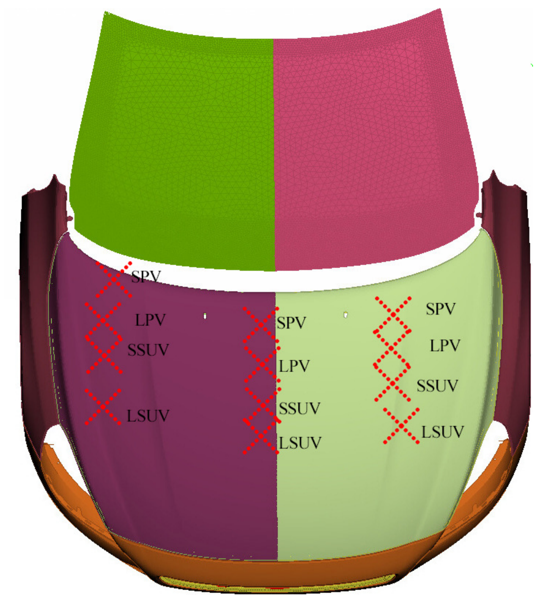

Figure 4.21: Head impact location on vehicle bonnet and windshield for 25km/h vehicle velocity, different vehicle types and impact points

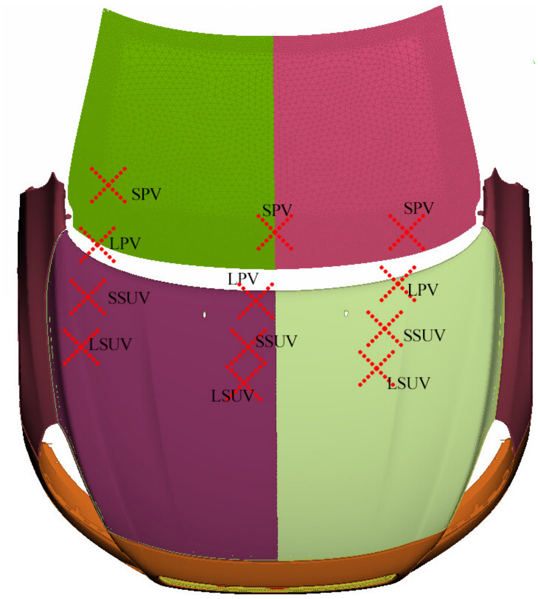

Figure 4.22: Head impact location on vehicle bonnet and windshield for 40km/h vehicle velocity, different vehicle types and impact points

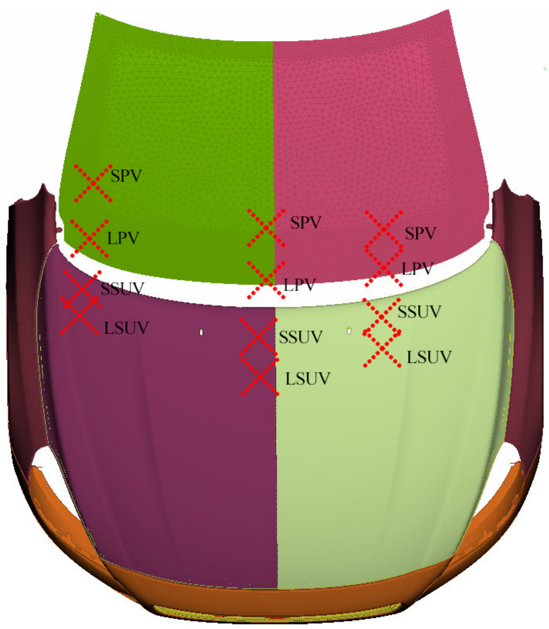

Figure 4.23: Head impact location on vehicle bonnet and windshield for 50km/h vehicle velocity, different vehicle types and impact points

For all the cases considered, it was observed that the impact location became higher and more backward from the bonnet top at low vehicle velocity circumstances (figure 4.21) to the windshield at high vehicle velocity circumstances (figure 4.23). A general trend shows that the head impact velocities to the vehicle front increased with increasing vehicle velocities. The head accelerations are mostly following the same trend, and the expectations are the cases of Small PV impacted at P1 and P5, Large PV impacted at P5 and Small SUV impacted at P5 under the vehicle velocity between 40 km/h and 50 km/h. The differences are mainly due to the clearance distance beneath the bonnet and the stiffness change of contact between the head and different vehicle structures.

All the 36 cases from the simulation matrix were analysed using the advanced KTH head model, and the summary of HIC_{15} and BrIC values calculated from both models is shown in Appendix 8.4.2. There are 6 cases which showed error terminations from either advanced or rigid head model simulations were excluded from the correlation analysis.

The correlation between HIC_{15} of THUMS model with rigid head and advanced KTH head was compared and plotted in figure 4.24. The data is not very well correlated ($R2<0.8$) and the data suggest that for the rigid head the HIC_{15} is about 92% of that of the deformable and advanced head.

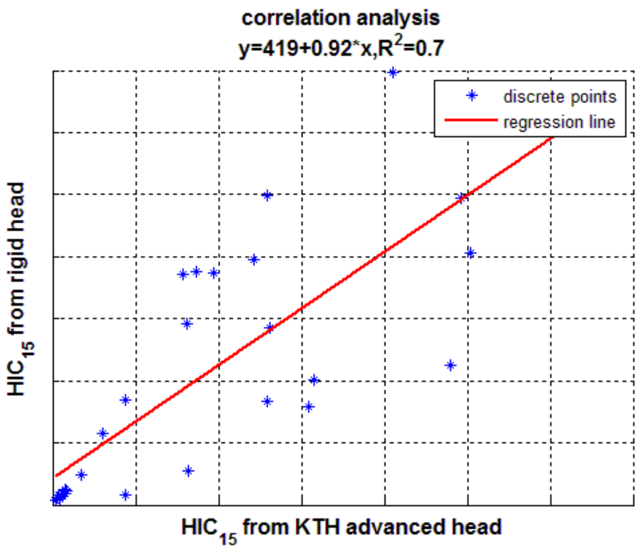

Figure 4.24: Correlation between HIC_{15} of advanced KTH head and HIC_{15} of rigid head

A comparison of the BrIC values from the THUMS model with rigid head and advanced head is made in order to investigate the correlation of criteria based on angular components. The result is as in figure 4.25. A closer linearized behaviour can be indicated with the R^2 value closer to 1 in BrIC analysis. , and the data between the two models are close to 100%.

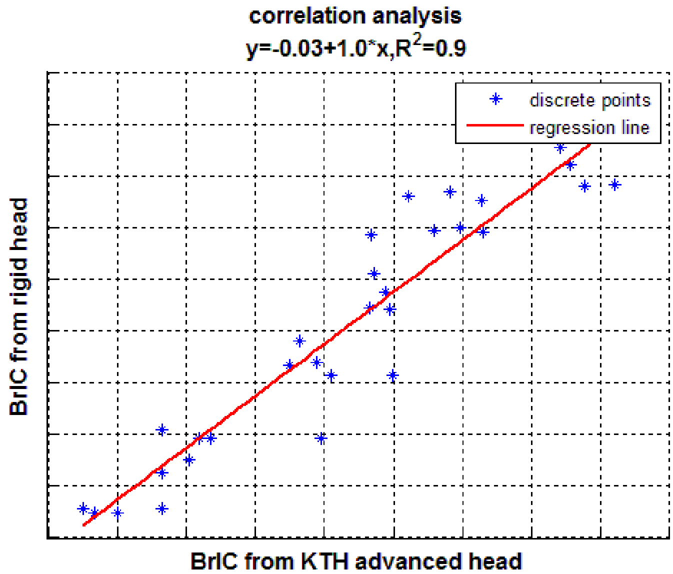

Figure 4.25: Correlation between BrIC from KTH advanced head and BrIC from rigid head

The AIS4+ brain injury probability versus BrIC were calculated for the simulations using the rigid and advanced KTH head. As requested by the company, the analysis data is not provided here in this report. A general trend of increasing probability of brain injury with increasing vehicle velocity is observed. On aspects of vehicle height, a Large SUV shows higher brain injury risk in all three velocity groups compared to the other types of vehicles.

The maximum principal strain (MPS) in the brain for vehicle velocities of 25km/h, 40km/h, and 50km/h and different impact points can be found in Appendix 8.4.4.

In general, the MPS values increases with increasing vehicle velocity. However, several head impact locations showed that with a lower impact speed, a high MPS value may occur depending on the region of vehicle where the head impacts. Figure 4.27 shows an example of the impact location P1 for a small PV under vehicle velocity of 25km/h, 40km/h, and 50km/h.

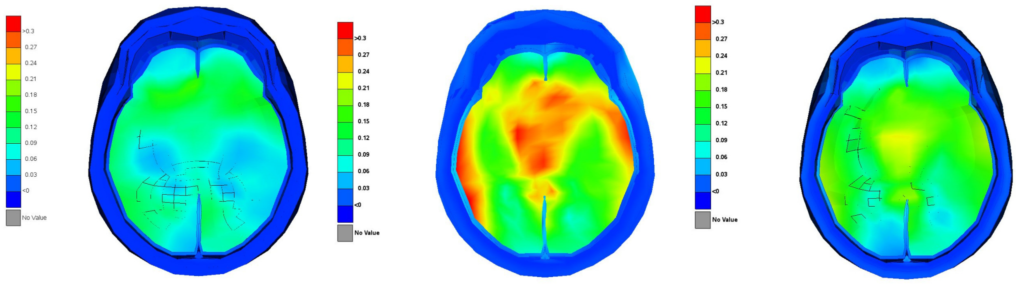

Figure 4.27: MPS in brain under 25km/h, 40km/h, and 50km/h with vehicle hitting the THUMS at the same location

4.3 Accident reconstructions

Accident reconstruction was carried out for two accident cases from real-life accidents.

Figure 4.28 shows the resultant linear accelerations of the head for reconstruction case 1 and case 2. Figure 4.29 shows the head impact location for the two cases.

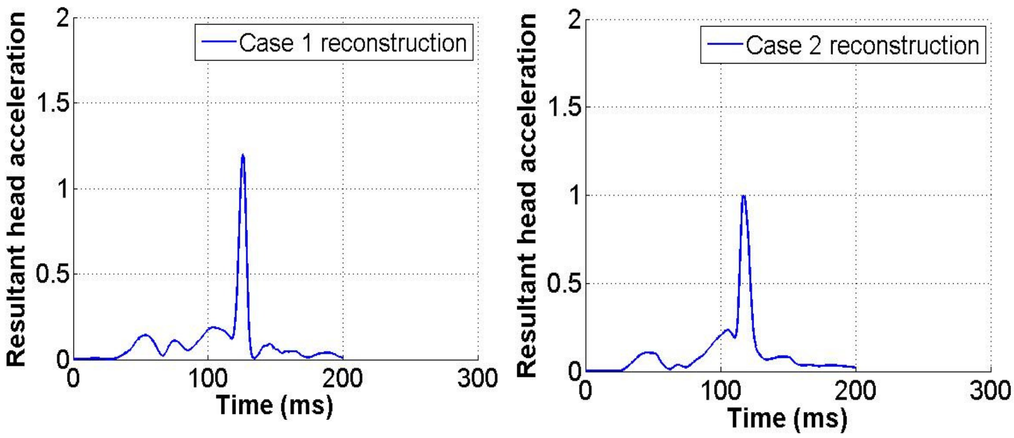

Figure 4.28: Resultant acceleration for case 1(left) and case 2(right)

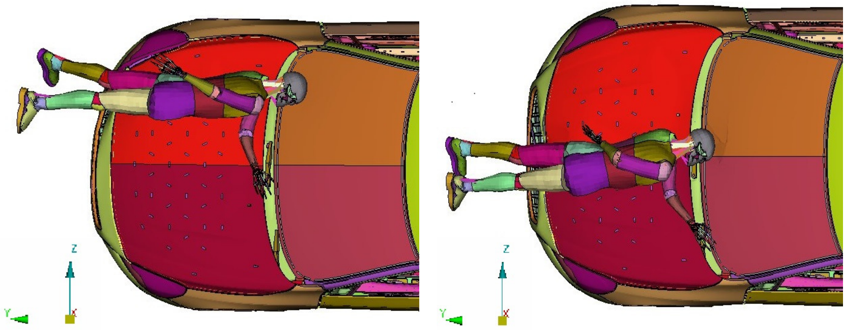

Figure 4.29: Head impact locations for case 1(left) and case 2(right)

The two reconstructed cases were based on categorizing the vehicle as large passenger vehicle. For both the cases the pedestrian head impacts the windshield near the cowl region. The information regarding the pedestrian location in front of vehicle during the impact for case 1 was missing in the accident database. Also, there were no post-accident images in the database which showed the impact location of the pedestrian, so an assumption was made for this data.

The resultant head impact velocity, resultant head linear acceleration and HIC_{15} value for the two reconstruction cases are presented in table 4.10.

Table 4.10: Maximum resultant head impact velocity, linear acceleration and HIC_{15} values for two reconstruction cases

Case no.	Vehicle impact velocity (km/h)	Resultant head impact velocity	Resultant head acceleration	HIC_{15}
Reconstruction case 1	50	0.89	1.20	1.14
Reconstruction case 2 (N)	50	1.00	1.00	1.00

The HIC_{15} as obtained is very high presenting a very high risk of injury to the head of pedestrian.

5 Discussion

In this chapter, the simulation results are discussed. Firstly, the results from simulations with the impactors are compared with those from simulations with THUMS. Secondly, the parameter study results are discussed. Lastly, accident reconstruction results are discussed.

5.1 Impactor-to-vehicle simulations with comparison of THUMS

As presented in the results section, a higher impact velocity will lead to more severe knee injuries in both Flex-PLI and THUMS. Though, none of the studied cases reached the thresholds of injuries defined for both models. Apart from it, no direct correlation can be drawn from the knee ligament elongation values as the difference of elongation data from Flex-PLI and THUMS are not comparable. One study by Miyazaki et al. [41] concluded that an impact height of 0 mm of the impactor showed a behaviour closer to that of THUMS, while a height of 75mm of the impactor had a better injury response correlation. In this study, the position of 75mm shows the highest ligament elongations due to the reason that the energy absorber was placed at the upper tibia region, thus comparatively low bending moment but more shearing. On the contrary, the position of walking stance has a knee joint impacting closer to the height of the bumper beam which causes less bending moment as well as shear displacement of the knee region with the deformation of the energy absorber on the bumper beam . As explained in the chapter 3.3, the ligament injury to the THUMS model is not analysed due to the change of shape and property of the element during the positioning process, and the poor behaviour in the impact simulations.

For comparison of bending moments of the tibia between Flex-PLI and THUMS, a small PV at different pedestrian impact locations and vehicle velocity of 40km/h was considered. The THUMS showed higher bending deformation for all cross-sections of tibia and all pedestrian impact points under same impact conditions as compared to Flex-PLI. Also, for this study, it was observed that overall the Flex-PLI when positioned at 0° inclination angle according to walking stance showed closer correlation in terms of maximum bending moments of different tibia cross-sections rather than when positioned 75mm above the ground level. The impact point P3 showed better correlation as compared to the other impact points. Also, the peak bending moments for Flex-PLI did not vary a lot for different impact points along energy absorber, however THUMS showed a lot of variation for different impact points for peak bending moments of different tibia cross-sections.

For head injuries, the THUMS model with KTH rigid head model shows the same trend and behaviour in terms of acceleration curve and impact duration. The correlation factor for HIC_{15} was R^2=0.80 and the x-coefficient for the regression was 0.62. This means that the two models do not correlate well in terms of HIC_{15} values because of the fact that for the THUMS model the head impact velocity is greater than actual vehicle velocity during impact which produced relatively high linear accelerations and hence HIC_{15} whereas for impactor the head impact velocity is similar to the vehicle velocity during the impact. Although, it was very interesting to see that the THUMS model and headform impactor produced approximately the same length of impact duration and trend starting from initial contact of head with the vehicle and ending at rebound of head, showing that there is correlation regarding modelling and behaviour between the two models. The brain injuries could not be compared with headform impactor used in EuroNCAP regulation tests due to absence of brain model in the impactor.

5.2 Vehicle-to-THUMS parameter study

A detailed vehicle-to-THUMS collision parameter study was conducted in the thesis. For the parameter study, vehicle height, vehicle velocity and pedestrian impact locations were varied.

The ligament injury analysis is feasible for and only for the vehicle with its default height due to the reason that the height of energy absorber was influenced when the vehicle height was varied with respect to BLE to mimic different vehicle types. In most of the THUMS simulations, ligament showed none or minor injuries. Such behaviour is undesired. The THUMS model being utilized has a changed stance from initial to walking, thus the position and the contact region between THUMS and vehicle also varies. Apart from that, changing of THUMS stance was not validated so the influence of ligament properties change (length, meshing shape and etc.) is not considered in this study. From the observation of the THUMS simulations, the knee showed a visible bending angle while the total elongation of MCL was low, as the shape of the MCL changed from a folded to an unfolded condition while no tension was detected.

Magnitude of bending moment of tibia bone was used as a measure to analyse injuries. It was observed that for all the cases the tibia-1 bending deformation was greater followed by tibia-2 bending deformation and tibia-3 bending deformation. Also, for 25km/h vehicle velocity and impact point P1, the tibia-1 bending moment was highest as compared to other impact points, the reason identified behind this is the direct implication of impact force on tibia-1 cross-section during vehicle-to-pedestrian collision and impact point P1 being near to the edge of the energy absorber which offers less deformation zone and less contact area for tibia. When vehicle-to-pedestrian impact velocity increases to 40km/h, the maximum bending deformation is observed in tibia-1 at impact point P1, reasons for higher bending moment being similar to the previous case. When the vehicle velocity further increases to 50km/h, the maximum bending deformation occurs for impact point P1 at tibia-1 cross-section due to contact near the edge of energy absorber.

If maximum bending deformation was compared according to different vehicle velocities at same impact points then it was observed that as the vehicle velocity increased the bending deformation increased for impact point P1. For impact point P3, the tibia-1 cross-section bending moment is higher at 25km/h and lower at 40km/h due to the fracture of femur at 40km/h impact velocity. Further, when the impact velocity increases, the bending moment increased significantly, showing that for higher velocities, the bending deformation is higher. For impact point P5, the overall trend was increase of bending deformation for different tibia-cross-sections with increasing vehicle velocities. Fracture of femur at 50km/h caused decrease in bending moment at this impact point.

For head injuries, HIC_{15} was used as measure. For analysis three simulations failed and were not analysed. The overall trend was for lower vehicle velocities, the risk of AIS3+ head injury was lower whereas for higher vehicle velocities, the AIS3+ head injury risk was higher. The head impact velocities increased with increasing vehicle velocities and was greater than vehicle velocity for most cases. The HIC_{15} value depended on the location of head impact on the vehicle and vehicle velocity. If the head impacted with hard parts beneath the bonnet or windshield around the cowl region, then the acceleration levels were high and the corresponding HIC_{15} values were high. Also, one more interesting fact as observed was that the THUMS shoulder first contacted the vehicle which already deformed the vehicle up to certain level before the head came into contact with the vehicle. Due to this there was less deformation zone provided for the head and it came almost into direct contact with the hard parts beneath the bonnet of the vehicle. Moreover, the THUMS model with an advanced head and neck KTH model contains a deformable brain and shows a more fluid-like manner, the influence of effective mass is considered to be the major factor for the higher HIC_{15} values exposed in the advanced KTH head.

Additional studies were conducted on the advanced KTH head, the MPS value being part of the studies. As presented by Bain et al. [42], the first stage of DAI can be identified when MPS value exceeds 0.2. Thibault et al. [43] explained in their study that a strain value of 0.3 can be considered as a threshold for severe DAI. The internal loading of brain can be observed by reading the MPS value in the advanced KTH head. From the parameter study results, the major reasons for the brain injury was found to be the contact pressure and the shear deformation caused by the rotation motion of the head. The damage in the brain regions are mostly located at corpus callosum, thalamus as well as the place where the skull is having direct contact with the vehicle structure where the linear acceleration translated into the cerebrum.

The study on BrIC indicates the possibility of using this injury criteria or other similar criteria which includes rotational components for a humanoid, while the correlation between this and ATD's needs consideration of more samples. Further, whether a rigid head or a detailed head model can have better injury prediction for real-life circumstances is still undecided. However, with the advanced KTH head it is possible to conduct analysis on the injuries caused by shear loading as well as the pressure diffusion inside the cerebrum. This is considered to be a merit comparing to the test dummy's head. On the contrary, a head with brain tends to have higher HIC_{15} values compared with a rigid head, which in the rating or the threshold may lead to a misunderstanding of the vehicle safety performance.

5.3 Accident reconstructions

For this study, two cases were reconstructed from the V_PAD accident database. Both the accident cases involved a large PV and vehicle velocity of 50km/h, lower leg injuries were not analysed as in this study a small PV was used to mimic a large PV and thus the bumper would not be accurately positioned for testing pedestrian safety. However, head injury analysis could be carried out as the location of head impact could be mimicked with such an approach of changing vehicle height to obtain different vehicle types. Since, the

THUMS model used was a 50^{th} percentile male model, so for both the reconstruction cases the head impact took place on the windshield near the cowl region but the pedestrian impact points and scenario were different. HIC_{15} values obtained represents high risk of severe head injury both to the skull and brain. These head injury level is high when compared to the one reported in the accident database. There are several factors which were not included in the simulations like the deceleration of the vehicle which might have been there in the real-world accident case, the running or walking speed of the pedestrian involved in the crash and the environmental conditions which could have led to differences in results as reported in accident database and the one obtained through FE simulations.

5.4 Pedestrian protection countermeasures

This section discusses the possible pedestrian protection countermeasures for the vehicle under study.

For preventing injuries to the lower leg, including a wider energy absorber would prove to be beneficial from pedestrian safety point of view as then the stiff parts of the vehicle could be better avoided during collision with a vehicle. For preventing injuries to the head and brain, including an active hood which rises up and pedestrian airbag would be useful as the region identified for an adult pedestrian as poor from design point of view is the cowl region around the windshield. If the hood rises up or pedestrian airbag is deployed then the pedestrian could avoid head impact with this area reducing the head and brain injury risk during vehicle-to-pedestrian collisions. Another possible solution could be allowing more deformation zone for the cowl region around the windshield.

5.5 Future studies

Future studies for the thesis include the use of advanced THUMS 4.0 model for assessing the injuries to the lower leg of the pedestrian. Also, the THUMS model used for this study was modified by including an advanced head and neck model from KTH and thus studying the lower leg injuries separately with a more advanced, flexible and original THUMS model would be interesting.

Further, scaling of THUMS model into different anthropometric sizes of female and child can be carried out to study the injuries to other group of pedestrians. For accident reconstructions, more cases can be analyzed to get an overall view of the correlation of injuries reported in the accident database and as predicted through simulations.

For analysis of brain injuries, other injury criteria like Cumulative Strain Damage Measure (CSDM) and Rotational Injury Criteria (RIC) could be interesting.

6 Conclusion

1. For knee ligament injuries, prediction by Flex-PLI and THUMS are not correlating.
2. THUMS predicted higher tibia bending deformation for tibia than Flex-PLI.
3. The tibia bending deformation as predicted by THUMS increased with increasing vehicle velocities and it decreased when the femur fractured.
4. Tibia-1 i.e. the upper tibia bending moment was higher for different vehicle velocities and pedestrian impact points.
5. Head linear accelerations as predicted by THUMS and headform impactor were in correlation to each other in terms of trend and behaviour of accelerations during impact.
6. For vehicle-to-THUMS simulations, most of the cases show low knee ligament elongation and high tiba-1 bending deformation.
7. The head impact velocities increased with increasing vehicle velocities.
8. The head impacted either the bonnet of the vehicle or windshield depending on the vehicle velocity and vehicle height.
9. For impact of lower leg at the edge of the energy absorber the risk of fracture for mid-tibia cross-section is low.
10. Injuries to the brain are higher for higher vehicle velocities and vice versa.
11. For higher head injury risk, the brain injury risk is high and vice versa
12. The accident reconstructions of the two cases through FE simulations showed injury risks higher than reported in the database.

7 References

[1] Natonal Highway Traffic Safety Administration (2012): *Traffic Safety facts*, U.S department of transportation, New Jersey, Washington D.C.

[2] Vezin P., Verriest J.P. (2005*): Development of a Set of Numerical Human Models for Safety*, pp. 1–16.

[3] European New Car Assessment Programme (2015): *Pedestrian Protection*, [Online]. Available: http://www.euroncap.com/en/vehicle-safety/the-ratings-explained/pedestrian-protection/

[4] Toyota Central R&D (2015): *Total Human Body Model for Safety (THUMS),* [Online]. Available: http://www.toyota.com/esq/safety/r-and-d/thums.html

[5] Kleiven S. (2002): *Finite Element Modelling of the Human Head,* Royal Institute of Technology*,* Sweden, ISSN 0280-4646.

[6] Lindman, M., (2011): *Pedestrians interacting with a passenger car; a study of real world accidents*, Ircobi Conference, pp. 255-264.

[7] Madymo Human Body Model Manual, Release 7.6 (2015): *TASS International.* pp. 7.

[8] European New Car Assessment Programme (2015): *EURO NCAP: For safer cars*, [Online]. Available: http://www.euroncap.com/en.

[9] European New Car Assessment Programme (2015): *EURO NCAP: Members and test facilities*, [Online]. Available: http://www.euroncap.com/en/about-euro-ncap/members-and-test-facilities/.

[10] European New Car Assessment Programme (2015): *How to read the stars*, [Online]. Available: http://www.euroncap.com/en/about-euro-ncap/how-to-read-the-stars/

[11] European New Car Assessment Programme (2015): *The ratings explained*, [Online]. Available: http://www.euroncap.com/en/vehicle-safety/the-ratings-explained/

[12] European New Car Assessment Programme (Euro NCAP): *Pedestrian testing protocol*, Version 8.0, 2014.

[13] European New Car Assessment Programme (Euro NCAP): *Assessment Protocol – Pedestrian Protection*, Version 8.0, 2014.

[14] European Enhanced Vehicle-safety Committee. (1998). *EEVC Working Group 17 Report—Improved Test Methods to Evaluate Pedestrian Protection Afforded by Passenger Cars.* Delft, the Netherlands: TN0 Crash-Sagety Research Centre, 6-8.

[15] Konosu, A., Issiki, T., Tanahashi, M., & Suzuki, H. (2007, June). *Development of a biofidelic flexible pedestrian legform impactor type GT (Flex-GT).* In Proceedings of the 20th International Technical Conference on the Enhanced Safety of Vehicles (pp. 18-21).

[16] Zander, O., Gehring, D. U., Lessman, P., & Bovenkerk, J. (2009). *Evaluation of a Flexible Pedestrian Legform Impactor (FlexPLI) for the Implementation within Legislation on Pedestrian Protection.* InPROCEEDINGS OF THE 21ST (ESV) INTERNATIONAL TECHNICAL CONFERENCE ON THE ENHANCED SAFETY OF VEHICLES, HELD JUNE 2009, STUTTGART, GERMANY.

[17] Kerrigan, J., Crandall, J. R., & Deng, B. (2008). *A new detailed multi-body model of the pedestrian lower extremity: Development and preliminary validation. In Proceedings of the International Research Council on the Biomechanics of Injury conference (Vol. 36, pp. 272-242).* International Research Council on Biomechanics of Injury.

[18] Tropiano, P., Thollon, L., Arnoux, P. J., Huang, R. C., Kayvantash, K., Poitout, D. G., & Brunet, C. (2004). *Using a finite element model to evaluate human injuries application to the HUMOS model in whiplash situation.* Spine, 29(16), 1709-1716.

[19] TOYOTA MOTOR CORPORATION & TOYOTA CENTRAL R&D LABS., INC. *User's Guide of Computational Human Model THUMS (Total Human Model for Safety) — AM50 Pedestrian Model: Version 1.4-060705*

[20] Fressmann D (2012): *Vehicle Safety using the THUMS^{TM} Human Model.* 11th German Ls-Dyna Forum 2012, October 9-10, 2012,Ulm Germany

[21] Yasuki, T., & Yamamae, Y. (2010). *Validation of kinematics and lower extremity injuries estimated by total human model for safety in SUV to pedestrian impact test.* Journal of Biomechanical Science and Engineering, 5(4), 340-356.

[22] Kleiven, S., & Hardy, W. N. (2002). *Correlation of an FE Model of the Human Head with Local Brain Motion--Consequences for Injury Prediction.* Stapp Car Crash Journal, (46), 123-44.

[23] Kleiven, S. (2006). *Evaluation of head injury criteria using a finite element model validated against experiments on localized brain motion, intracerebral acceleration, and intracranial pressure.* International Journal of Crashworthiness, 11(1), 65-79

[24] Giordano, C., & Kleiven, S. (2014). *Connecting fractional anisotropy from medical images with mechanical anisotropy of a hyperviscoelastic fibre-reinforced constitutive model for brain tissue.* Journal of The Royal Society Interface, 11(91), 20130914.

[25] Copes WS, Sacco WJ, Champion HR, Bain LW (1990): *Progress in Characterising Anatomic Injury.* Proceedings of the 33rd Annual Meeting of the Association for the Advancement of Automotive Medicine, Baltimore, MA, USA, pp. 205-218.

[26] Association for the Advancement of Automotive Medicine (2005): *Abbreviated Injury Scale Manual,* first edition.

[27] Woo S. L., Debski R. E., Withrow J. D., and Janaushek M. A. (1999): *Current Concepts Biomechanics of Knee Ligaments,* Vol. 27, No.4, pp. 533-543.

[28] Albert I. King (2000): *Fundamental of Impact Biomechanics: Part-I Biomechanics of the Head, Neck and Thorax*, Annual Review of Biomedical Engineering, Vol.2, August 2000, pp. 55-81.

[29] Schmitt K.U., Neiderer P., Muser M. and Walz F. (2010): *Trauma Biomechanics – Accidental Injury in Traffic and Sports*, Springer, Zurich.

[30] Kerrigan, J., Drinkwater, D.C., Kam, C.Y., Murphy, D.B., Ivarsson, B.J., Crandall, J.R., Patrie, J. (2008). *Tolerance of the Human Leg and Thigh in Dynamic Latero-Medial Bending, ICRASH 2004.*

[31] Yong Peng et al. (2012): *A study of kinematics of adult pedestrian and head impact conditions in case of passenger car collisions based on real world accident data*. IRCOBI conference. pp 766-788.

[32] Takhounts Erik G. (2013): *Development of Brain Injury Criteria (BRIC)*, National Highway Traffic Safety Administration, Stapp Car Crash Journal, Vol. 57, Novemeber 2013,pp. 243-266.

[33] Davidsson J. (2015): *Global Head Injury Criteria*, Chalmers University of Technology, SAFER, Göteborg, Sweden, March 2015.

[34] Morén, D., & Pehrs, G. (2013). *Study of Vehicle-to-Pedestrian Interactions with FEM–Evaluation of Upper Leg Test Methods using a Human Body Model.*

[35] Implementation of virtual testing in safety regulations (IMVITER): *Final Report Summary* [Online]. Available: http://cordis.europa.eu/result/rcn/55811_en.html.

[36] Implementation of Virtual Testing in safety Regulations (IMVITER), *Analysis of New Simulation Technologies for Pedestrian Safety . Potential of VT to Fully Substitute RT for this Purpose.* vol. D6.1, pp. 1–48, 2012.

[37] Zander, O., Gehring, D. U., Lessman, P., & Bovenkerk, J. (2009). *Evaluation of a Flexible Pedestrian Legform Impactor (FlexPLI) for the Implementation Within Legislation on Pedestrian Protection.* PROCEEDINGS OF THE 21ST (ESV) INTERNATIONAL TECHNICAL CONFERENCE ON THE ENHANCED SAFETY OF VEHICLES, HELD JUNE 2009, STUTTGART, GERMANY.

[38] CHAWLS, A., Mukherjee, S., Mohan, D., & Parihar, A. (2004). *Validation of lower extremity model in THUMS.* In PROCEEDINGS OF THE IRCOBI-INTERNATIONAL RESEARCH COUNCIL ON THE BIOMECHANICS OF IMPACT CONFERENCE HELD SEPTEMBER 2004, GRAZ, AUSTRIA.

[39] Martinez, L., Guerra, L., & Compigne, S. (2008). *Influence of vehicle shape and stiffness on the pedestrian lower extremity injuries: Review of current pedestrian lower leg test procedure.* In Proceedings of the International Research Council on the Biomechanics of Injury conference (Vol. 36, pp. 243-258). International Research Council on Biomechanics of Injury.

[40] Brian G. McHenry (2004): *Head Injury Criterion and the ATB*, ATB user's group, 2004, 5 pp.

[41] Miyazaki, H., Matsuoka, F., Kuwahara, M., Kitagawa, Y., & Yasuki, T. (2009). *Development of Flexible Pedestrian Legform Impactor FE model and Comparative study with Leg Behavior of Human FE Model THUMS.* 21st ESV, 09-0112.

[42] Bain, A. C., & Meaney, D. F. (2000). *Tissue-level thresholds for axonal damage in an experimental model of central nervous system white matter injury.* Journal of biomechanical engineering, 122(6), 615-622.

[43] Thibault, L. E., Gennarelli, T. A., Margulies, S. S., Marcus, J., & Eppinger, R. (1990). *The strain dependent pathophysiological consequences of inertial loading on central nervous system tissue.* In International IRCOBI Conference on the Biomechanics of Impacts, 1990, Bron, France.

8 Appendix

8.1 Simulation Matrix

A) THUMS KTH model with rigid head

Simulation no.	Vehicle model	BLE height (mm)	Vehicle speed (km/h)	Impact point
1	Small PV	694	40	P1
2	Small PV	694	40	P3
3	Small PV	694	40	P5
4	Large PV	768	40	P1
5	Large PV	768	40	P3
6	Large PV	768	40	P5
7	Small SUV	877	40	P1
8	Small SUV	877	40	P3
9	Small SUV	877	40	P5
10	Large SUV	988	40	P1
11	Large SUV	988	40	P3
12	Large SUV	988	40	P5
13	Small PV	694	25	P1
14	Small PV	694	25	P3
15	Small PV	694	25	P5
16	Large PV	768	25	P1
17	Large PV	768	25	P3
18	Large PV	768	25	P5
19	Small SUV	877	25	P1
20	Small SUV	877	25	P3
21	Small SUV	877	25	P5
22	Large SUV	988	25	P1
23	Large SUV	988	25	P3
24	Large SUV	988	25	P5
25	Small PV	694	50	P1
26	Small PV	694	50	P3
27	Small PV	694	50	P5
28	Large PV	768	50	P1
29	Large PV	768	50	P3
30	Large PV	768	50	P5
31	Small SUV	877	50	P1
32	Small SUV	877	50	P3
33	Small SUV	877	50	P5
34	Large SUV	988	50	P1
35	Large SUV	988	50	P3
36	Large SUV	988	50	P5

B) THUMS KTH model with advanced head

Simulation no.	Vehicle model	BLE height (mm)	Vehicle speed (km/h)	Impact point
37	Small PV	694	40	P1
38	Small PV	694	40	P3
39	Small PV	694	40	P5
40	Large PV	768	40	P1
41	Large PV	768	40	P3
42	Large PV	768	40	P5
43	Small SUV	877	40	P1
44	Small SUV	877	40	P3
45	Small SUV	877	40	P5
46	Large SUV	988	40	P1
47	Large SUV	988	40	P3
48	Large SUV	988	40	P5
49	Small PV	694	25	P1
50	Small PV	694	25	P3
51	Small PV	694	25	P5
52	Large PV	768	25	P1
53	Large PV	768	25	P3
54	Large PV	768	25	P5
55	Small SUV	877	25	P1
56	Small SUV	877	25	P3
57	Small SUV	877	25	P5
58	Large SUV	988	25	P1
59	Large SUV	988	25	P3
60	Large SUV	988	25	P5
61	Small PV	694	50	P1
62	Small PV	694	50	P3
63	Small PV	694	50	P5
64	Large PV	768	50	P1
65	Large PV	768	50	P3
66	Large PV	768	50	P5
67	Small SUV	877	50	P1
68	Small SUV	877	50	P3
69	Small SUV	877	50	P5
70	Large SUV	988	50	P1
71	Large SUV	988	50	P3
72	Large SUV	988	50	P5

8.2 Knee ligament elongation curves

8.2.1 Flex-PLI knee ligament elongation curves

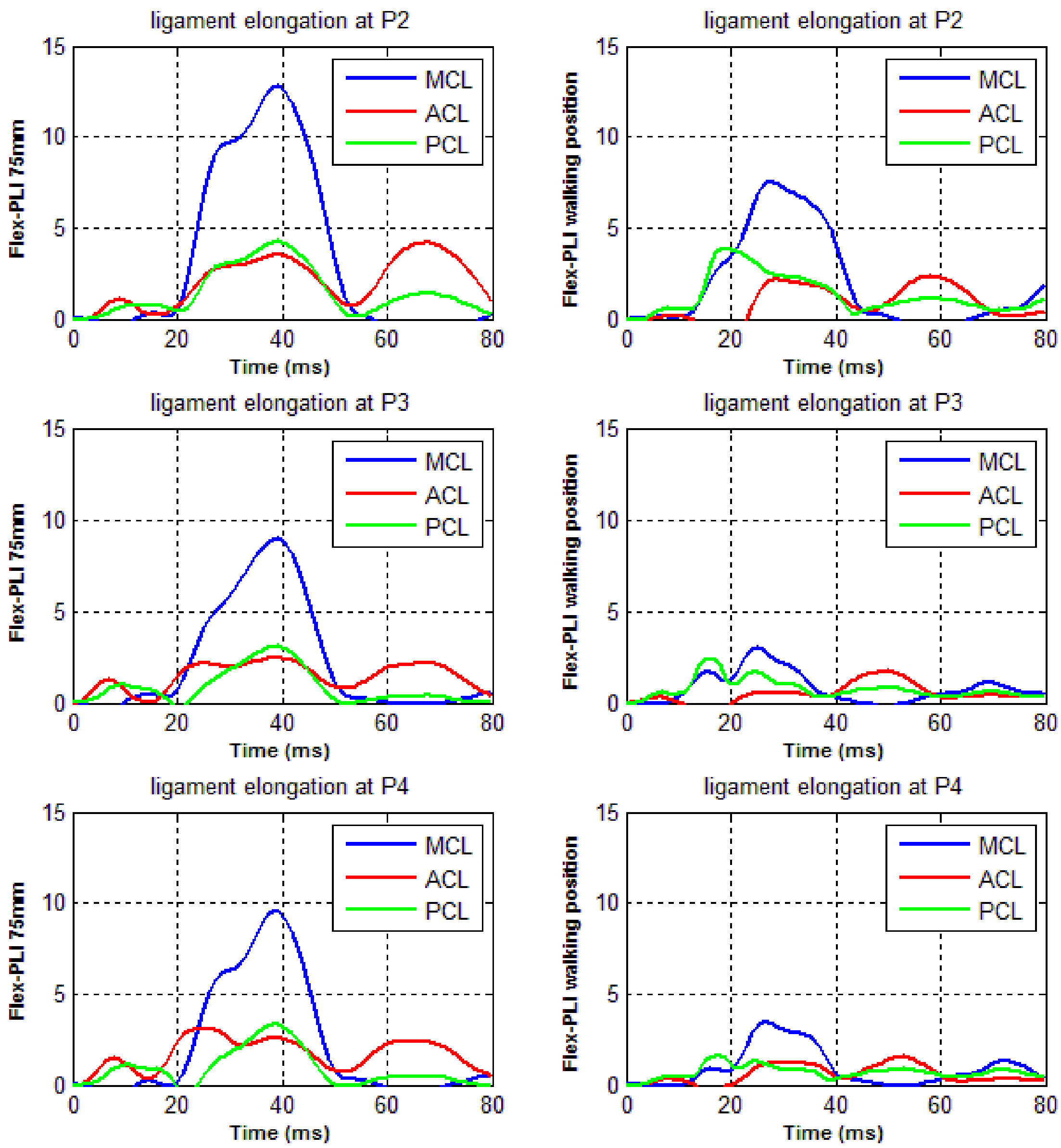

8.2.2 Vehicle-to-THUMS knee ligament elongation curves compared for different velocities with variation of impact points

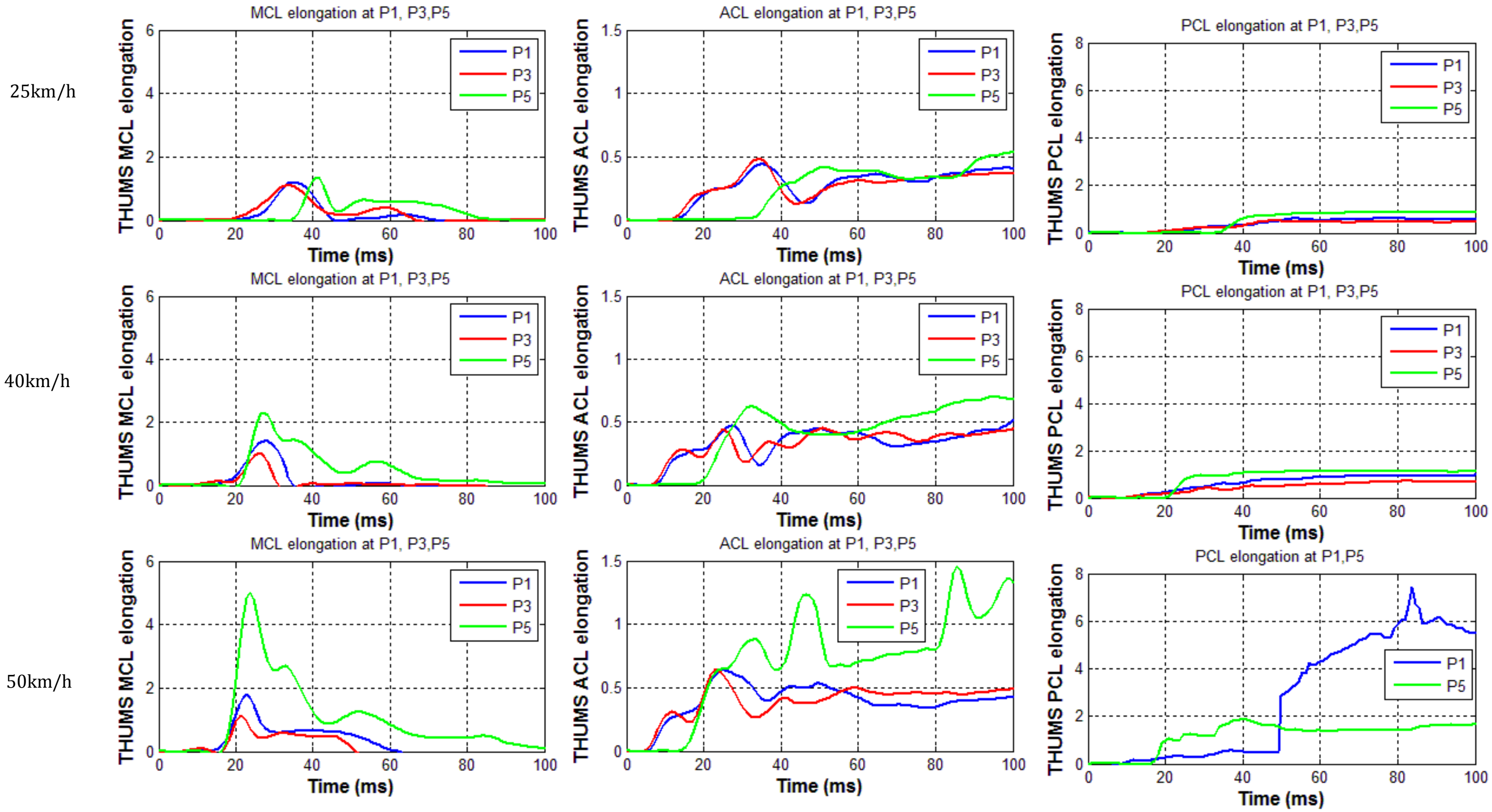

8.2.3 Vehicle-to-THUMS knee ligament elongation curves compared for different impact points with variation of vehicle velocities.

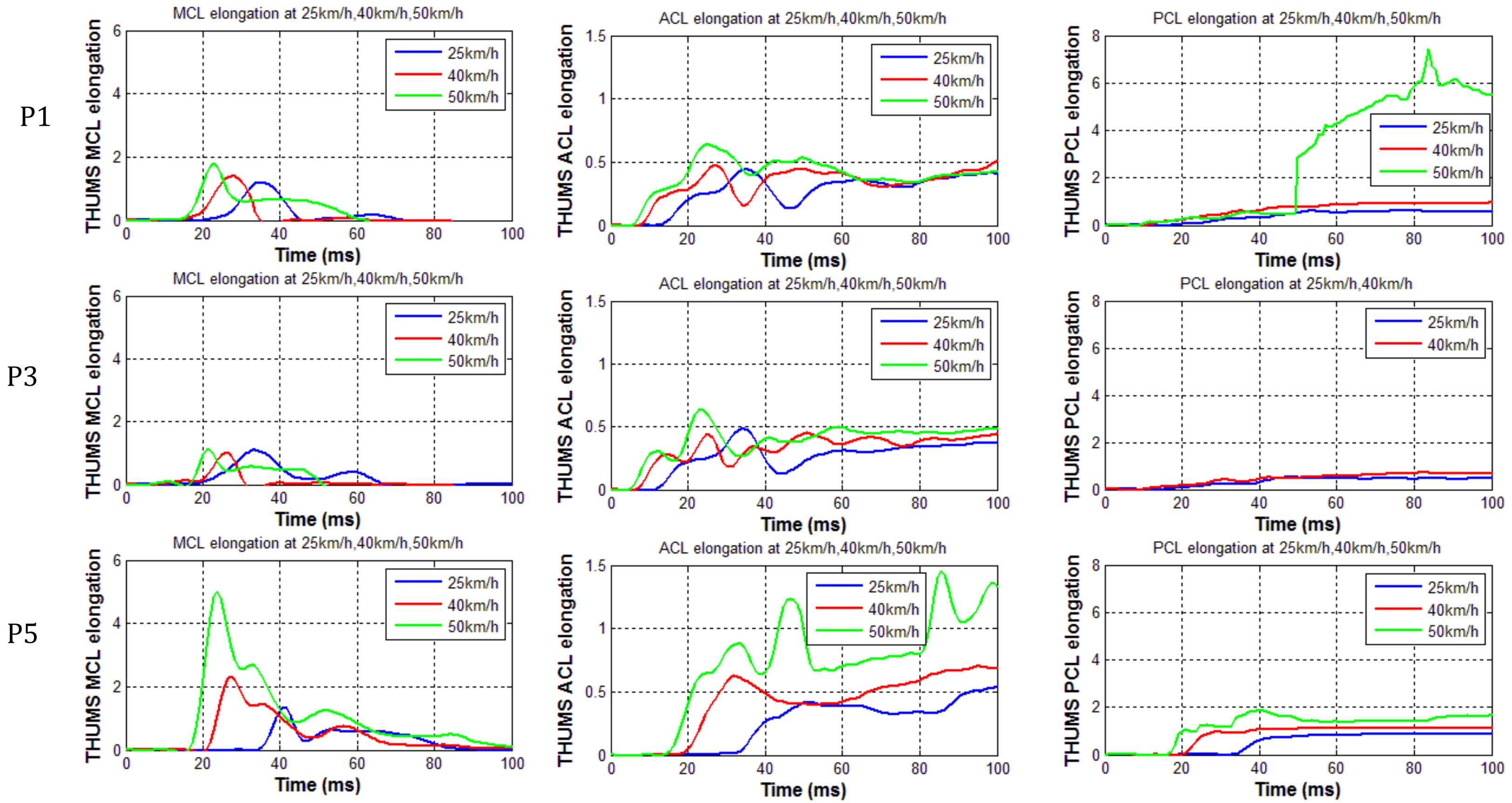

8.3 Tibia Resultant bending moment Curves

8.3.1 Comparison of resultant bending moment for different tibia cross-sections between THUMS and Flex-PLI at different impact points.

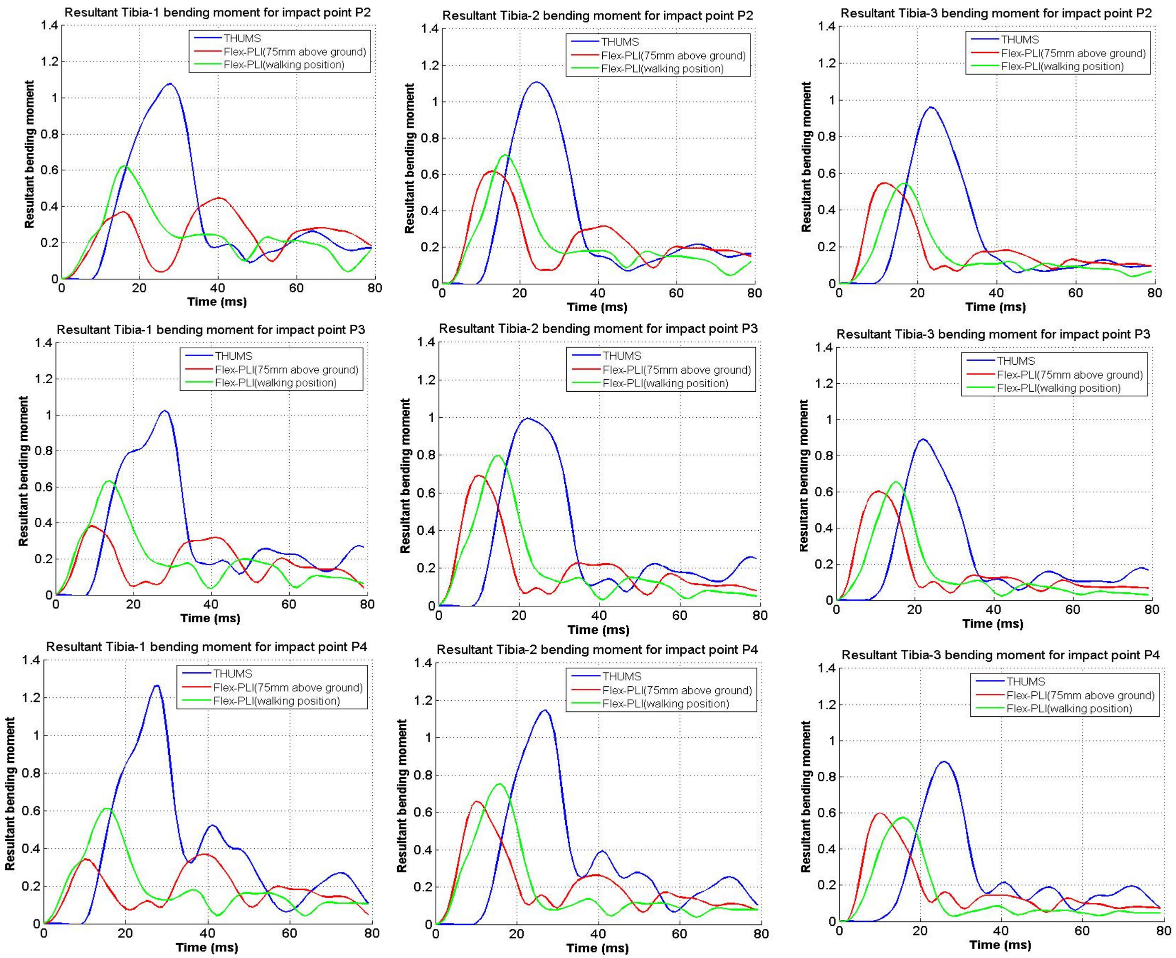

8.3.2 Resultant bending moment of different tibia cross-sections for different vehicle velocities with variation of impact points.

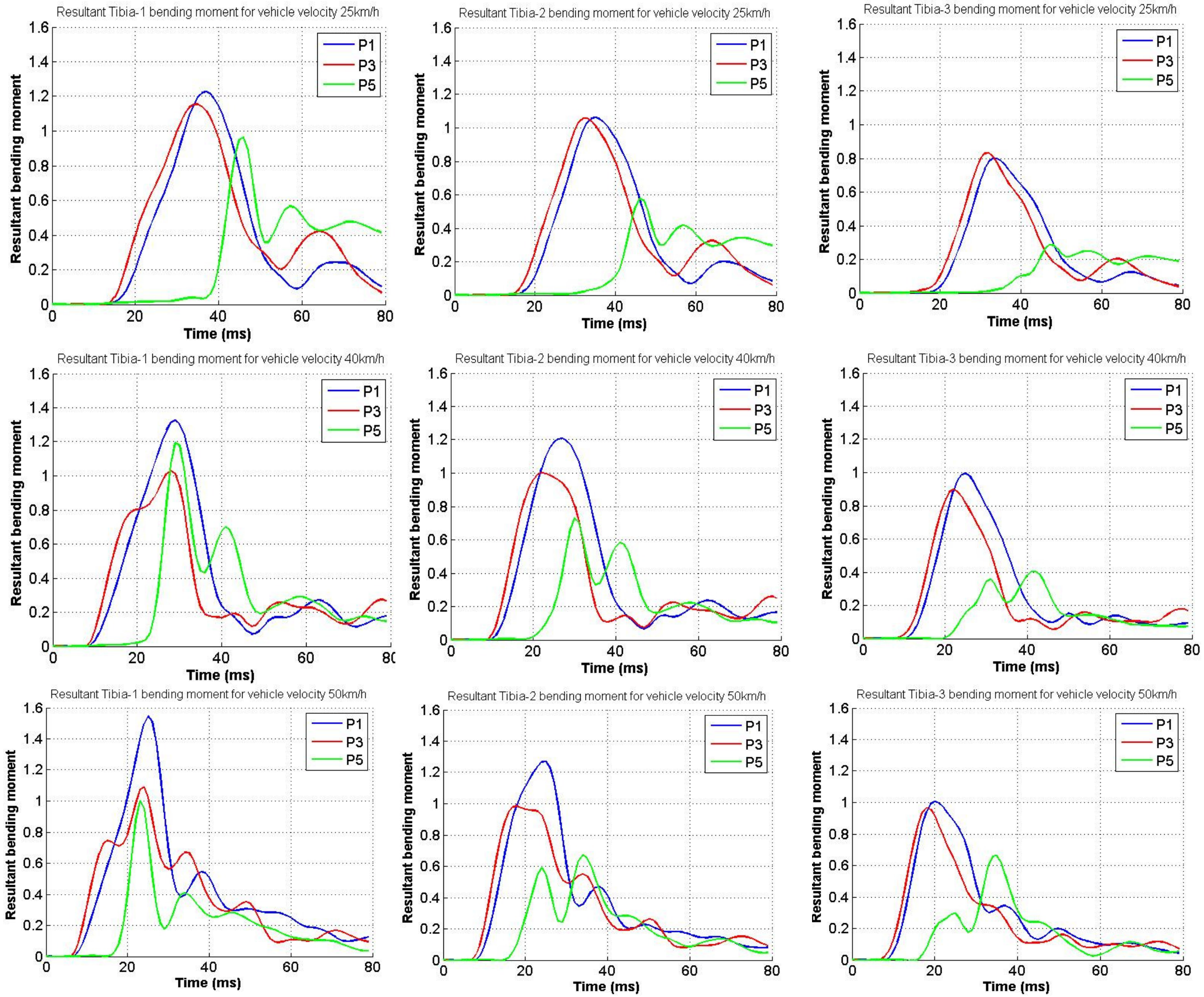

8.3.3 Resultant bending moment of different tibia cross-sections for different impact points with variation of vehicle velocities.

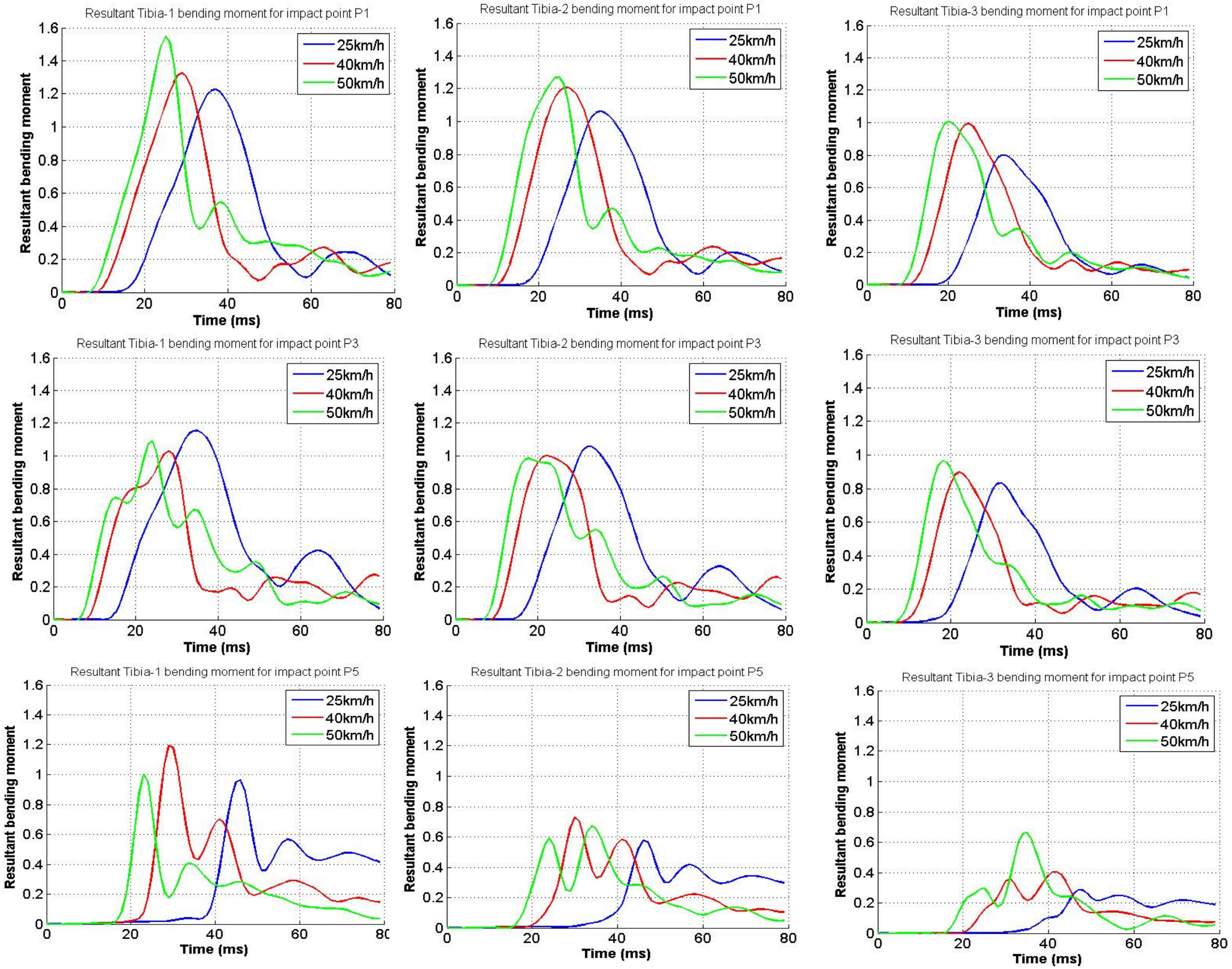

8.4 Head and Brain

8.4.1 Head impact velocity and head resultant linear acceleration curves for different vehicle velocities and impact points.

Small PV

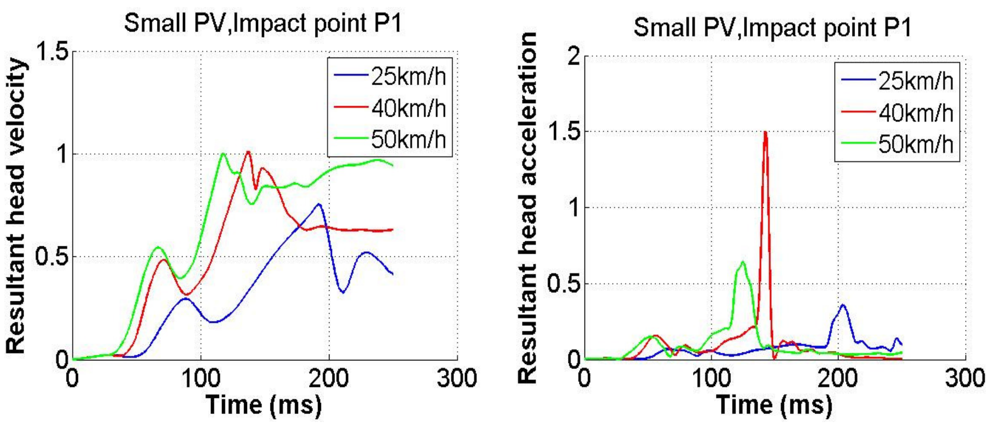

Figure 8.1 Resultant head impact velocity (left) and resultant head acceleration (right) for impact point P1

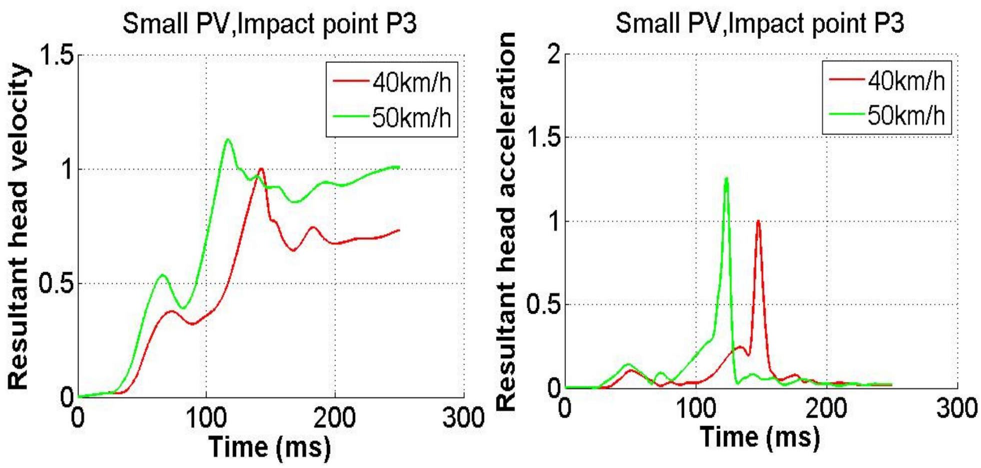

Figure 8.2: Resultant head impact velocity (left) and resultant head acceleration (right) for impact point P3

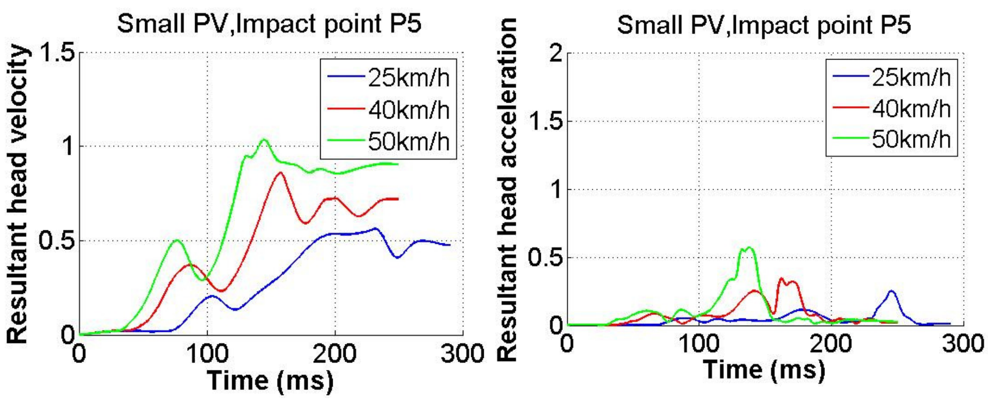

Figure 8.3: Resultant head impact velocity (left) and resultant head acceleration (right) for impact point P5

Large PV

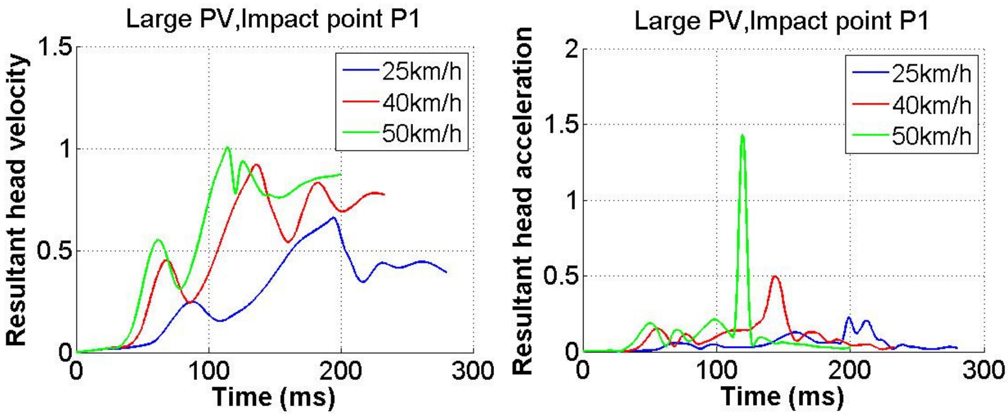

Figure 8.4: Resultant head impact velocity (left) and resultant head acceleration (right) for impact point P1

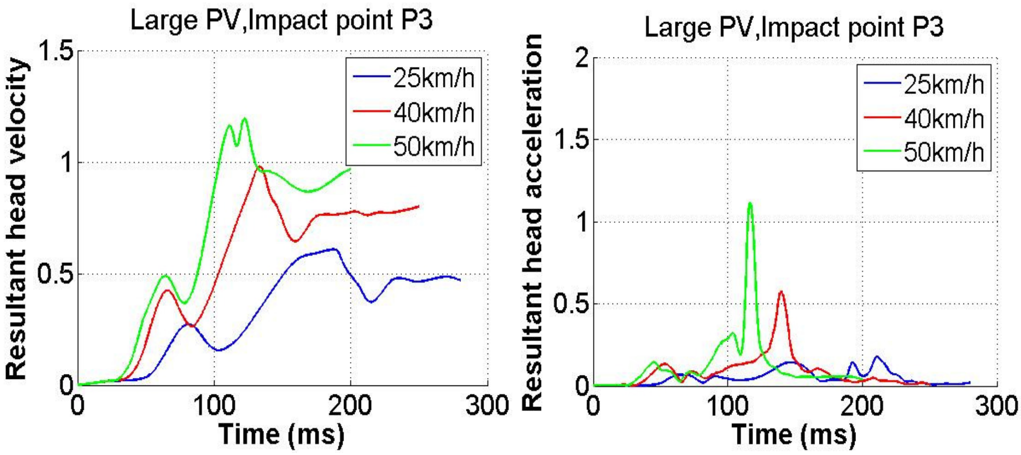

Figure 8.5: Resultant head impact velocity (left) and resultant head acceleration (right) for impact point P3

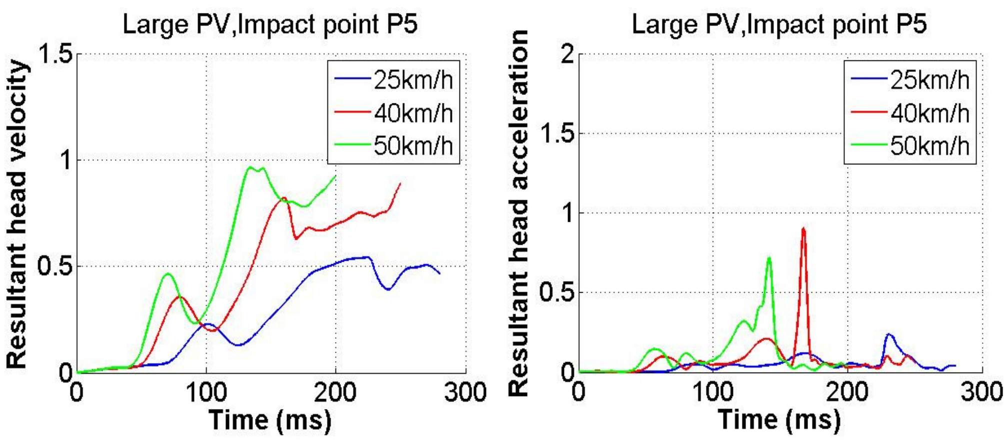

Figure 8.6: Resultant head impact velocity (left) and resultant head acceleration (right) for impact point P5

Small SUV

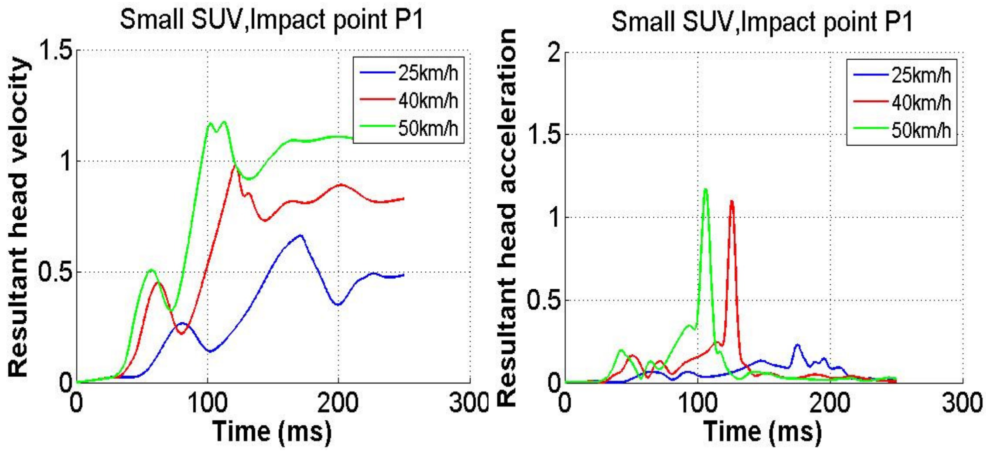

Figure 8.7: Resultant head impact velocity (left) and resultant head acceleration (right) for impact point P1

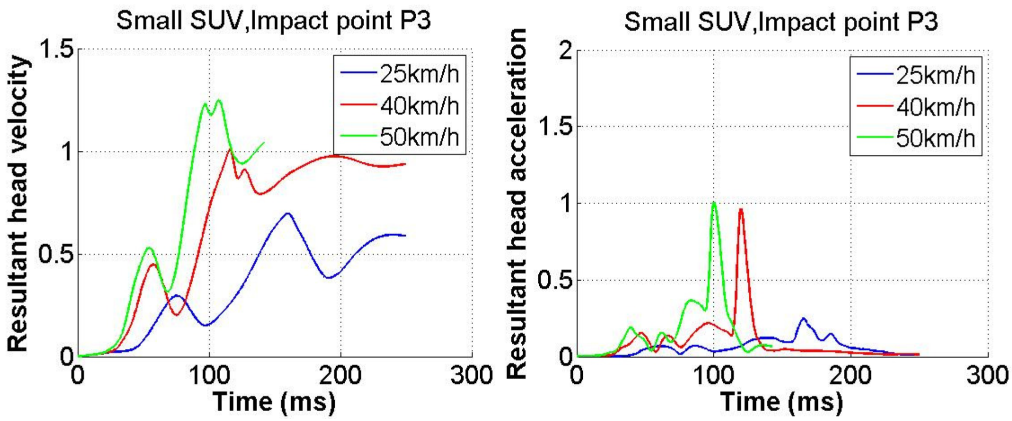

Figure 8.8: Resultant head impact velocity (left) and resultant head acceleration (right) for impact point P3

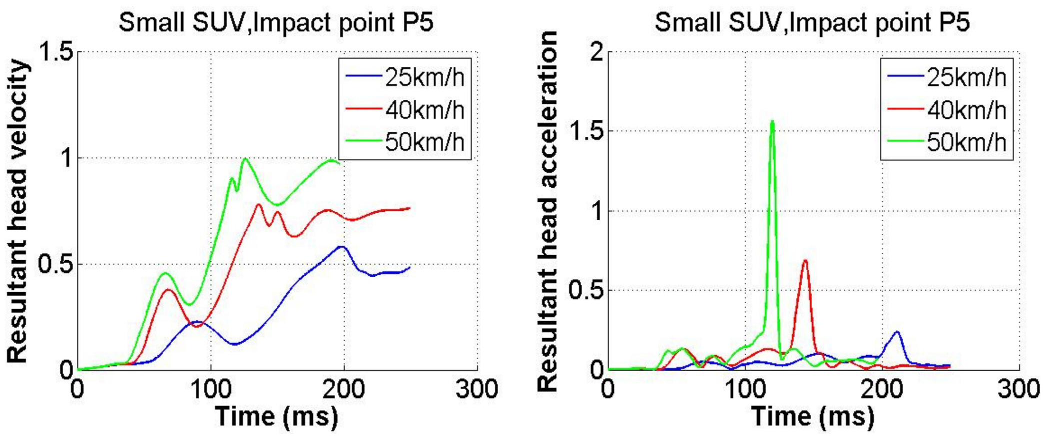

Figure 8.9: Resultant head impact velocity (left) and resultant head acceleration (right) for impact point P5

Large SUV

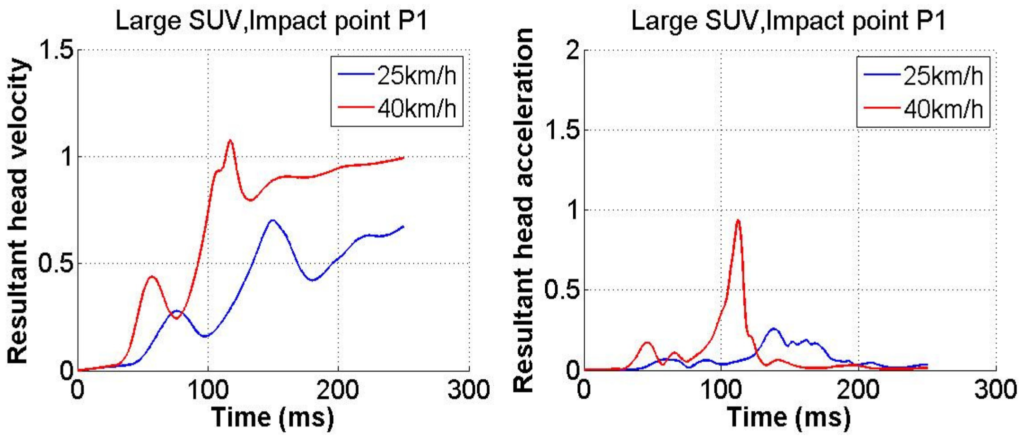

Figure 8.10: Resultant head impact velocity (left) and resultant head acceleration (right) for impact point P1

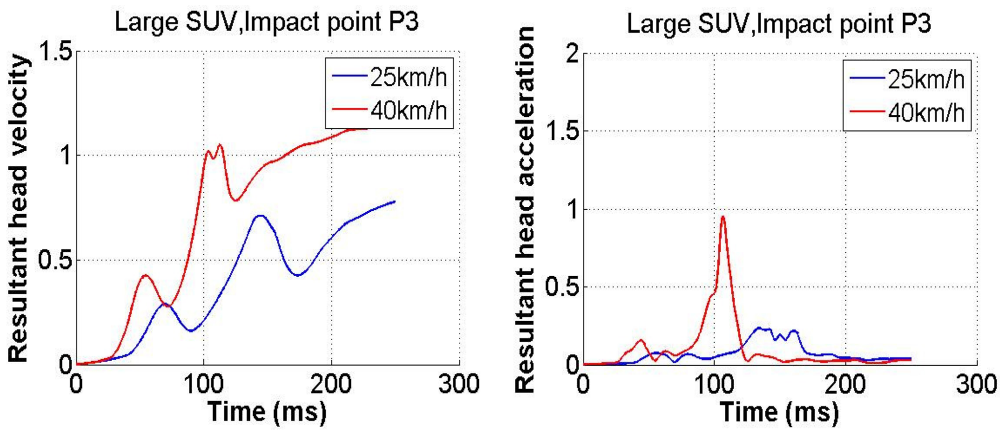

Figure 8.11: Resultant head impact velocity (left) and resultant head acceleration (right) for impact point P3

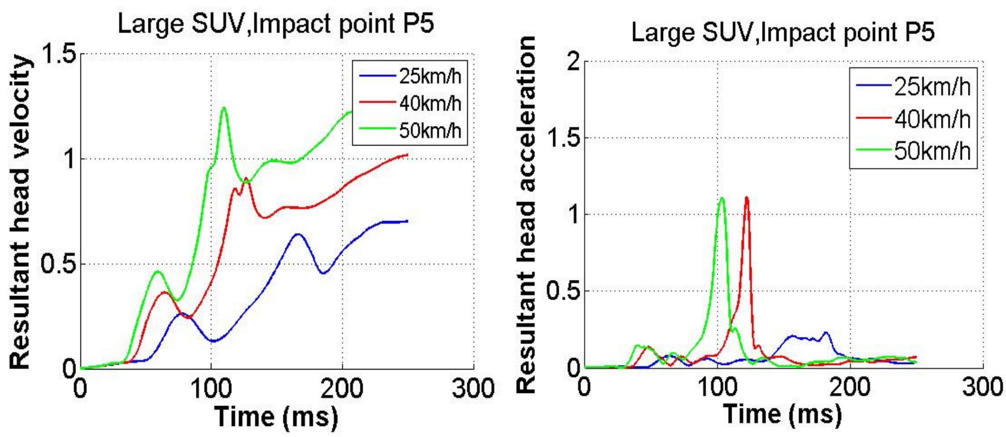

Figure 8.12: Resultant head impact velocity (left) and resultant head acceleration (right) for impact point P5

8.4.2 HIC15 and BrIC values from THUMS model with rigid head and THUMS wih advanced KTH head.

a) HIC_{15} and BrIC calculated from THUMS with rigid head

Simulation no.	Vehicle model	Vehicle speed (km/h)	Impact point	HIC_{15}	BrIC
1	Small PV	40	P1	2.33	1.11
2	Small PV	40	P3	1.00 (N)	1.00 (N)
3	Small PV	40	P5	0.19	0.87
4	Large PV	40	P1	0.36	0.98
5	Large PV	40	P3	0.41	0.97
6	Large PV	40	P5	0.58	0.74
7	Small SUV	40	P1	1.18	0.96
8	Small SUV	40	P3	1.02	0.97
9	Small SUV	40	P5	0.60	0.74
10	Large SUV	40	P1	1.31	1.19
11	Large SUV	40	P3	1.32	1.23
12	Large SUV	40	P5	1.31	1.26
13	Small PV	25	P1	0.17	0.61
14	Small PV	25	P3	error	error
15	Small PV	25	P5	0.06	0.61
16	Large PV	25	P1	0.04	0.68
17	Large PV	25	P3	0.02	0.74
18	Large PV	25	P5	0.05	0.60
19	Small SUV	25	P1	0.04	0.70
20	Small SUV	25	P3	0.06	0.75
21	Small SUV	25	P5	0.05	0.60
22	Large SUV	25	P1	0.09	0.85
23	Large SUV	25	P3	0.08	0.87
24	Large SUV	25	P5	0.06	0.85
25	Small PV	50	P1	0.79	1.11
26	Small PV	50	P3	1.74	1.17
27	Small PV	50	P5	0.71	1.03
28	Large PV	50	P1	2.20	1.18
29	Large PV	50	P3	1.43	1.10
30	Large PV	50	P5	0.56	0.91
31	Small SUV	50	P1	1.76	1.12
32	Small SUV	50	P3	1.39	1.19
33	Small SUV	50	P5	2.45	1.17
34	Large SUV	50	P1	error	error
35	Large SUV	50	P3	error	error
36	Large SUV	50	P5	2.16	1.44

b) HIC15 and BrIC calculated from KTH advanced head

Simulation no.	Vehicle model	Vehicle speed (km/h)	Impact point	HIC_{15}	BrIC
37	Small PV	40	P1	2.22	1.08
38	Small PV	40	P3	0.92	1.01
39	Small PV	40	P5	0.58	0.88
40	Large PV	40	P1	error	error
41	Large PV	40	P3	0.21	0.99
42	Large PV	40	P5	0.91	0.78
43	Small SUV	40	P1	error	error
44	Small SUV	40	P3	0.57	1.02
45	Small SUV	40	P5	0.31	0.93
46	Large SUV	40	P1	0.68	1.32
47	Large SUV	40	P3	0.61	1.26
48	Large SUV	40	P5	0.55	1.25
49	Small PV	25	P1	0.12	0.71
50	Small PV	25	P3	0.10	0.77
51	Small PV	25	P5	0.05	0.61
52	Large PV	25	P1	0.02	0.71
53	Large PV	25	P3	0.02	0.76
54	Large PV	25	P5	0.04	0.62
55	Small SUV	25	P1	0.03	0.75
56	Small SUV	25	P3	0.04	0.71
57	Small SUV	25	P5	0.02	0.65
58	Large SUV	25	P1	0.05	0.94
59	Large SUV	25	P3	0.06	0.92
60	Large SUV	25	P5	0.31	1.02
61	Small PV	50	P1	1.69	1.14
62	Small PV	50	P3	1.73	1.04
63	Small PV	50	P5	1.11	1.00
64	Large PV	50	P1	2.38	1.10
65	Large PV	50	P3	1.77	1.00
66	Large PV	50	P5	1.09	0.90
67	Small SUV	50	P1	0.91	1.11
68	Small SUV	50	P3	0.85	1.28
69	Small SUV	50	P5	1.44	1.14
70	Large SUV	50	P1	1.44	1.5155
71	Large SUV	50	P3	1.44	1.4954
72	Large SUV	50	P5	error	error

8.4.3 Maximum principal strain in brain for different vehicle velocities and impact points.

Vehicle model	THUMS position	Brain Injury (25km/h)	Brain Injury (40km/h)	Brain Injury (50km/h)
Small PV	P1	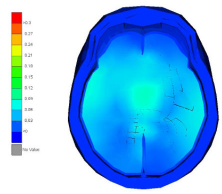	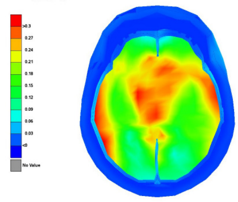	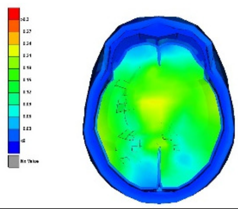
Small PV	P3	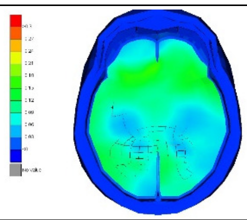	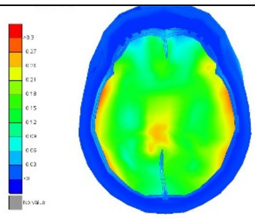	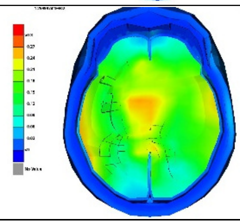
Small PV	P5	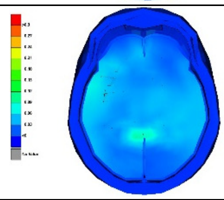	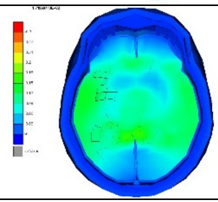	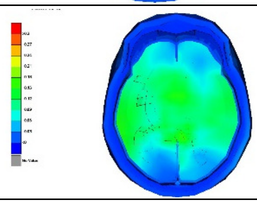
Large PV	P1	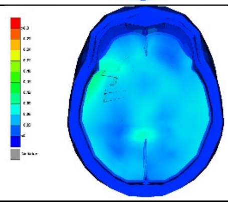	Error	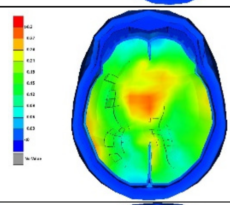
Large PV	P3	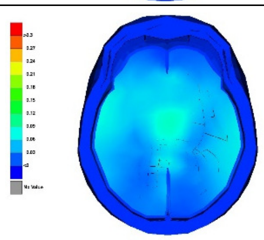	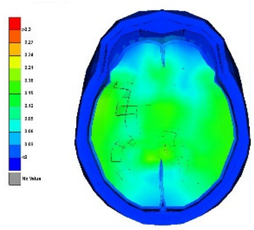	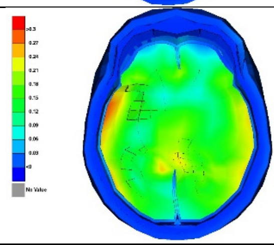
Large PV	P5	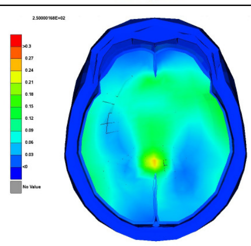	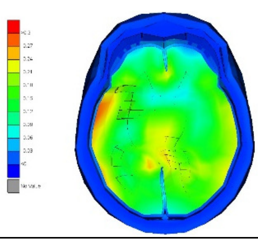	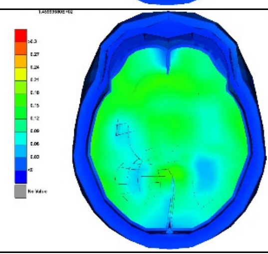
Small SUV	P1	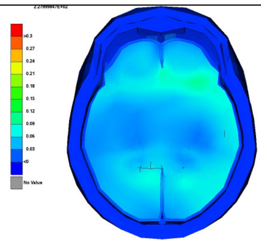	Error	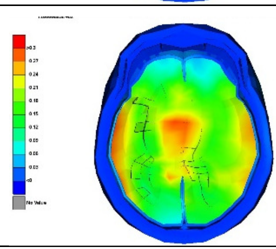

Smal l SUV	P3	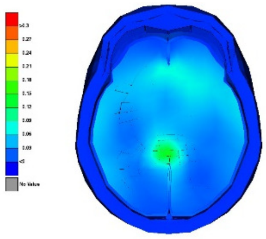	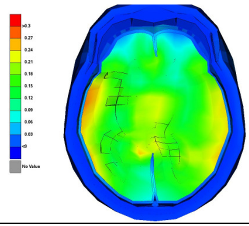	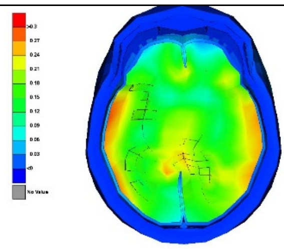
Smal l SUV	P5	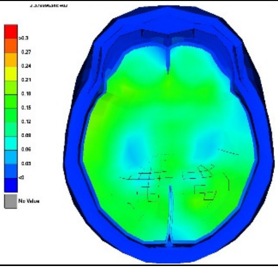	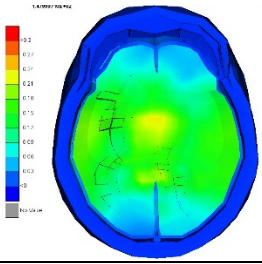	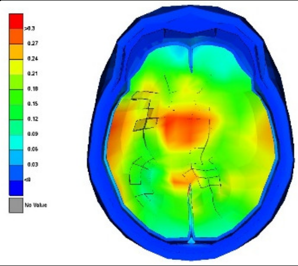
Larg e SUV	P1	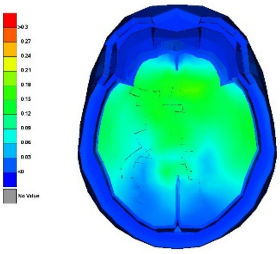	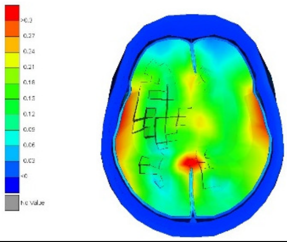	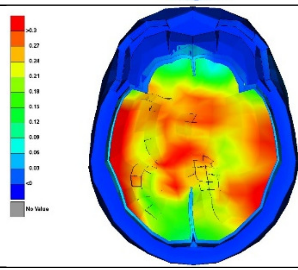
Larg e SUV	P3	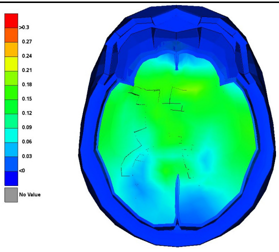	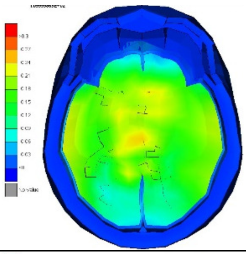	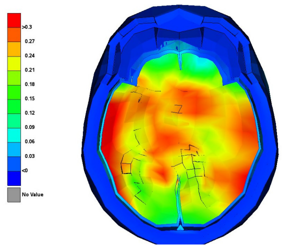
Larg e SUV	P5	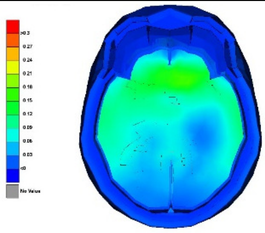	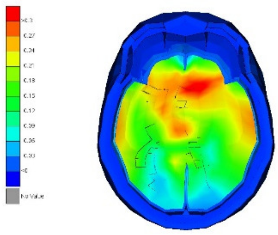	error